Xenosiderophore transporter gene expression and clade-specific filamentation in *Candida auris* killifish infection

Hugh Gifford[a], Tina Bedekovic[a], Nicolas Helmstetter[a], Jack Gregory[a], Qinxi Ma[a], Alexandra C. Brand[a], Duncan Wilson[a], Johanna Rhodes[b,c], Mark Ramsdale[a], Tetsuhiro Kudoh[d,1], Rhys Farrer*[a,1]

Abstract

Candida auris is an emerging infectious agent and World Health Organisation (WHO) critical priority fungal pathogen. Rising drug resistance, massive nosocomial outbreaks and diagnostic challenges complicate clinical treatment, resulting in a patient mortality rate of ~45%. A critical bottleneck in understanding virulence is the lack of gene expression profiling models during *in vivo* host tissue infection. To understand transcriptional responses during in-host infection, we developed a thermo-relevant fish embryo yolk-sac microinjection model (*Aphanius dispar*; Arabian killifish; AK) at human body temperature, featuring clinically relevant features of host immunity. This allowed us to interrogate infection dynamics through dual host-pathogen RNA-seq at 24 and 48 h post injection (HPI) at 37 °C across the five major clades (I-V) of *C. auris*. Host gene expression following infection indicated features of heat shock, complement activation, and nutritional immunity, including haem oxygenase (*HMOX*) expression in response to clade IV infection. We identified an *in vivo* transcriptional signature across five clades of *C. auris* that was highly enriched for putative xenosiderophore transmembrane transporters. We describe this newly-discovered seventeen-member xenosiderophore transporter candidate (*XTC*) family in terms of individual gene expression patterns, and a sub-clade of five putative haem transport-related (*HTR*) genes, also up-regulated during infection. Only the basal clade V isolate formed

filaments during infection, coinciding with typical and atypical regulators of morphogenesis, including *UME6*, *HGC1*, and the novel adhesin *SCF1*. Clades I and IV demonstrated increased virulence, coinciding with up-regulation of three *HTR* genes in clade IV, and the mating-type locus (*MTL*) non-mating gene *PIKA* in both. Our study provides critical insights into the pathogenesis of *C. auris*, including species-wide up-regulation of *XTC* and *HTR* genes during clinically relevant *in vivo* host tissue infection.

Keywords: *Candida auris*, virulence, gene expression, transcriptome, pathogenicity, Arabian killifish, *Aphanius dispar*, siderophore transport, mating-type locus, filamentation

[a]MRC Center for Medical Mycology, University of Exeter, Geoffrey Pope Building, Stocker Road, Exeter, United Kingdom, EX4 4QD

[b]Department of Medical Microbiology, Radboudumc, Geert Grooteplein Zuid 10, Nijmegen, Netherlands, 6525 GA

[c]MRC Centre for Global Infectious Disease Analysis, Imperial College London South Kensington Campus, London, United Kingdom, SW7 2AZ

[d]Biosciences, University of Exeter, Geoffrey Pope Building, Stocker Road, Exeter, United Kingdom, EX4 4QD

[1]Co-Senior Author

*Corresponding Author - R.Farrer@exeter.ac.uk

Introduction

C. auris is an ascomycetous yeast in the *Metschnikowiaceae* family that has rapidly transitioned from recent emergence to global public health threat[1] and World Health Organisation (WHO) critical priority human fungal pathogen[2]. Despite the oldest known historical isolate dating from 1996[3], the first formal species identification occurred in 2008[4]. Within ten years, *C. auris* had caused nosocomial outbreaks around the world, with high rates of azole antifungal drug resistance and a rising incidence of

58 pan-drug resistance[5]. These factors required extreme measures including Intensive
59 Care Unit (ICU) shutdowns and massive infection control costs[6–8]. Worryingly, *C. auris*
60 is now a leading cause of invasive candidiasis in several hospital settings globally[9,10].
61 Distinct clades of *C. auris*, including a sixth clade identified and described in
62 publications only in 2024[11,12], indicate the simultaneous emergence of multiple lineages
63 that are highly adapted for human infection[13,14]. The clinical impact, phenotypic traits
64 and simultaneous emergence of multiple clades of *C. auris* underscore the urgency to
65 understand its mechanisms of pathogenicity.
66
67 The factors governing in-host fitness and virulence during infection are poorly
68 understood. *C. auris* bloodstream infection is associated with a crude mortality of
69 ~45%[15]. Virulence factors in other distantly related *Candida* species, such as
70 *C. albicans*, include hypha-mediated invasion[16], the invasin Als3[17], and the secreted
71 toxin, candidalysin[18]. In contrast, *C. auris* has been shown to reproduce as budding
72 yeasts in mammalian tissues[19,20]. Although *C. auris* possesses multiple adhesins
73 associated with an aggregation phenotype[21,22], there has been no evidence of toxin
74 synthesis[23,24]. *C. auris* evades host immune responses through cell surface masking[25],
75 secreted aspartyl protease digestion of host tissue[26], and intra-phagocytic survival with
76 cell lysis[27]. Clades I, III, and IV are more commonly associated with invasive disease
77 and nosocomial outbreaks, while clades II and V have been primarily reported in cases
78 of otomycosis and rarely in bloodstream infection[28]. Human mortality associated with
79 *C. auris* candidaemia is potentially higher with clades I and IV than clade III, but this
80 difference has not been shown to be statistically significant[29]. Clade and strain-specific
81 genotypic and phenotypic variation may underlie differences in clinical presentation and
82 pathogenesis.
83
84 Gene expression profiling *in vivo vs in vitro* conditions has become a standard
85 approach for assessing host and pathogen responses to infection. To date, no
86 experiment has described the gene expression of *C. auris* or its host during *in vivo*
87 infection of living tissue. Studies assessing the transcriptome in an *in vivo* catheter

88 model[30], human whole blood *ex vivo*[31], co-incubation with human dermal fibroblasts[32] or
89 murine cell line-derived macrophages[33] have been useful, but the bottleneck for
90 pathogen gene expression is for profiling infection of *in vivo* living tissue. Additionally,
91 host responses have been assessed in murine peripheral skin[34], human peripheral
92 blood-derived monocytes[35] and murine bone marrow-derived macrophages[36]. However,
93 these studies have not reported adequate pathogen RNA recovery to interrogate
94 pathogen DNA expression in-host, except for the dual RNA-seq study using the *ex vivo*
95 whole blood model, for which it was possible to compare gene expression profiles
96 between *C. auris* and other *Candida* species.
97
98 The dearth of studies profiling host-pathogen gene expression *in vivo* for *C. auris*
99 infection may relate to the lack of a model which allows adequate RNA recovery,
100 balanced with a reasonable degree of clinical relevance. Most murine models, such as
101 BALB/c[19,37–39] and C57BL/6 mice[36], have only very rarely demonstrated lethality through
102 *C. auris* infection[35,40,41] without major immunosuppression with
103 cyclophosphamide/cortisone[42–53], monoclonal antibody neutrophil depletion[20,54], or other
104 immunodeficiency[21,55,56]. Additionally, mouse models are also expensive and associated
105 with concerns over environmental pathogen shedding[57]. Alternative host models such
106 as *Galleria mellonella*[37,47,58–64], *Drosophila melanogaster*[65] and
107 *Caenorhabditis elegans*[63] have been employed, but these may lack key elements of
108 mammalian-relevant immune systems, thus limiting their scope of application. In
109 patients, immune control of *C. auris* is thought to depend on myeloid cell activity *via* C-
110 type lectin receptors such as complement receptor 3 and mannose receptor MMR,
111 followed by interleukin (IL)-17 pathway activation[66,67]. Therefore, an animal model that
112 aligns with these mechanisms is required for human-relevant profiling of host-pathogen
113 interactions.
114
115 Fish larvae must survive hostile and varied ocean environments, demonstrating
116 very early innate immune responses such as antimicrobial peptide production and the
117 complement cascade[68,69]. Only in adulthood are teleost fish expected to possess

118 functional IL-17 subtypes (A and F) that lead to T-helper-17 subset differentiation and
119 adaptive immunity in response to fungal infection[70]. The zebrafish (*Danio rerio*) model
120 has allowed hindbrain[25,71] and swim bladder[72] microinjection modelling of *C. auris*
121 infection, but rarely at temperatures above 30 °C, which zebrafish are broadly intolerant
122 of. Again, we are unaware of any in-host transcription studies using the zebrafish
123 model. Fungal transcriptional programmes can vary greatly across temperatures and
124 are critical for mammalian pathogenesis[73–75]. A thermotolerant teleost fish embryo
125 model such as the *Aphanius dispar*, also known as the Arabian killifish (AK), which can
126 acclimatise to temperatures up to and including 40 °C[76–79] offers a balance between
127 considerations of suitability for experimental manipulation and applicability to human
128 fungal infection at mammalian temperatures.
129
130 Additionally, though the environmental origins of *C. auris* have not been
131 conclusively demonstrated, a marine origin has been hypothesised and supported by
132 successful isolation of *C. auris* in coastal waters of both Indian and Pacific oceans[80,81].
133 Notably, a close relative of *C. auris* in the *Metschnikowiaceae* clade, *C. haemulonii*, was
134 first isolated in 1961 from the gut of blue-striped grunt (genera name "*Haemulon*" for
135 their blood-red mouth interior)[82]. Therefore, a marine model could shed light on a
136 possible evolutionarily adaptive niche relevant not only to human infection but also to
137 hypothetical origins in an emerging pathogen. Additionally, fish embryo models align
138 with the principles of replacement, refinement and reduction of animals in laboratory
139 research and offer a opportunity to develop novel clinically relevant models with ethical
140 benefits over models such as adult mice[83].
141
142 In this paper, we present the first study exploring in-host virulence of *C. auris*
143 clades I-V in the AK yolk-sac microinjection model at 37 °C. We supplemented our
144 validation of the model with histology, fungal burden recovery, and dual host-pathogen
145 RNA-seq. By comparing *in vivo* and *in vitro* expression profiles of *C. auris*, we detected
146 a cross-clade expression signature that was significantly enriched for siderophore
147 transporter *SIT1* paralogues, which mediate uptake of siderophores produced by other

148 microbes (xenosiderophores). We designated this expanded gene family as
149 xenosiderophore transporter candidates (*XTC*), which included a haem transport-related
150 (*HTR*) sub-clade. We also identified *in vivo* filamentation by clade V during infection,
151 which was associated with orthologues of key hypha-associated genes from
152 *C. albicans*. Together, these findings substantially enhance our knowledge of the
153 processes employed by *C. auris* during infection.
154

155 ## Results

156

157 ### *C. auris* clades I-V are virulent in the AK microinjection model and clade V
158 ### uniquely exhibits in-host filamentation

159

160 Microinjection of the AK yolk-sac with each of the five *C. auris* clades was lethal
161 at 37 °C (91.7-100% 7-day mortality for each clade) compared to sham injection (5.6%
162 mortality). Kaplan-Meier survival curves demonstrated a significantly earlier lethality for
163 clade I (*vs* II, III or V, $p < 0.001$) and clade IV (*vs* II or III, $p < 0.04$) (**Fig. 1A**; **Table S1**).
164 Growth of the clade II strain in YPD-broth at 37 °C was noticeably slower over 24 h
165 compared with other clades (**Fig. S1A**). However, colony-forming units (CFU) recovered
166 post-infection from AK embryos were commensurate with similar in-host growth (**Fig.**
167 **1B**), with no differences identified between clades immediately post injection ($\bar{x}$ = 673
168 CFUs per infected embryo), 24 h post injection (HPI) ($\bar{x}$ = 1.12 x10^5) or 48 HPI ($\bar{x}$ = 1.78
169 x10^5), except for a lower CFU in clade V compared to clade III at 48 HPI ($\bar{x}$ 4.48 x10^5 *vs*
170 1.56 x10^4, $p < 0.01$). These results indicate that AK embryo yolk-sac microinjection is a
171 suitable model for the study of lethal *C. auris* infection at mammalian temperature.
172

173 Histological sectioning of the AK yolk-sac at 48 HPI revealed budding yeast
174 morphologies, except for the clade V strain, which demonstrated predominantly
175 filamentous forms (**Fig. 1C**). Lower CFUs in clade V could therefore be explained by
176 increased aggregation of filamentous cells. When grown in YPD-broth before

177 microinjection, all isolates exhibited yeast morphologies; clade V colonies recovered
178 from AK yolk-sac infection and grown on YPD-agar demonstrated rough (as opposed to
179 smooth) colonies in approximately 1-2% of plated colonies (**Fig. S1B**), which consisted
180 of elongated yeast cells and filamentous structures (> 10-50 μm) reminiscent of
181 pseudohyphae (**Fig. S1C**). Death was defined by cessation of heartbeat, which was
182 followed by yolk-sac collapse visible by timelapse microscopy (**Fig. 1D**). These findings
183 informed the study design for comparing *C. auris* gene expression between individual
184 clades during *in vivo* and *in vitro* growth to detect drivers of phenotypic and
185 morphological variation relevant to in-host virulence (**Fig. 1E**).
186

187 ## *C. auris* triggered host iron-nutritional immunity, heat shock response, and
188 complement activation

189

190 To determine whether microinjection interefered with host transcriptional
191 responses, we identified differentially expressed genes (DEGs) between sham injection
192 and no injection, defined as genes with significant ± >2 log-fold change in expression
193 after multiple testing. Though principle components analysis did not separate gene
194 expression profiles (**Fig. S1D**), correlation clustering separated sham injection and
195 negative controls without injection (**Fig. S1E**). However, there were only 30 DEGs for
196 sham injection compared to no injection (0.11% detected genes; **Fig. 2A**), with up-
197 regulation of zero and seven genes (at 24 and 48 HPI, respectively) and down-
198 regulation of four and nineteen genes (24 and 48 HPI, respectively). Four GO terms
199 were significantly enriched in the set of genes up-regulated at 48 HPI (relating to
200 sarcomere generation, organisation, M-band and muscle) with no enriched KEGG
201 pathways or PFAM domains, according to a falsed discovery rate (FDR) cut-off of
202 0.001. These GP terms were driven exclusively by three orthologues of murine *TITIN*
203 (log-fold change $\bar{x}$ = 7.59, gene ratio 0.16), a ~ 3-4 MDa cardiac muscle protein with a
204 putative role in haemodynamic stress tolerance and volume overload mechano-sensing
205 (**Fig. 2B**). Other up-regulated genes included vascular adhesion molecules and
206 hypothetical immunomodulator, dipeptidase 1 (*DPEP1*, **Table S2**). High survival of AK

207 embryos receiving sham injection and minor changes in gene expression (consistent
208 with physiological responses to exogenous fluid bolus) supported continued analysis of
209 host responses to infection.
210
211 To characterise host responses to *C. auris* during infection, we identified host
212 DEGs between infection by each clade and sham injection. Principle components
213 analysis (**Fig. S1D**) and correlation clustering (**Fig S1F**) did not cluster gene expression
214 profiles separately at either time-point (24 and 48 HPI). We identified 685 DEGs during
215 infection with any clade (2.49% potential genes), of which 183 were up-regulated and
216 508 were down-regulated in response to at least one clade. There were no DEGs
217 shared in common across host responses to all five clades, and only a small set of four
218 up-regulated genes and one down-regulated gene shared across host responses to four
219 clades of infection (**Table S2**). Up-regulated genes included Laminin subunit alpha-1
220 (*LAMA1*, not significant in response to clade III) and three genes that were not
221 significant in response to clade II, Glucose-6-phosphatase (*G6PC*), DN117939
222 (hypothetical protein) and Tryptophan aminotransferase protein 1 (*TAR1*);
223 immunoglobulin-like fibronectin type III domain-containing protein 1 (*IGFN1*) was down-
224 regulated. These results suggest AK larvae have a subtle and non-uniform response to
225 each clade of *C. auris* microinjection at these time-points, also reflecting levels of
226 virulence and stages of infection.
227
228 We identified clade-specific AK responses to infection. At 24 HPI, clade II elicited
229 the greatest host response, with up-regulation of 41 genes and down-regulation of 210
230 genes (**Fig. 2A**). However, at 48 HPI, clade IV elicited the greatest response (49 up-
231 regulated, 104 down-regulated). Heat shock proteins (*HSP30* and *HSP70*, but not
232 *HSP90*), complement cascade elements, pattern recognition receptors (PRRs),
233 inflammatory transcription regulators, and modulators of nutritional immunity were
234 differentially expressed with higher log-fold changes in clades I and IV, especially at
235 48 HPI (**Fig. 2C**). The most prominent gene relevant to pathogen recognition was
236 *CARD14* in clade I and IV infection at 48 HPI (**Fig. 2D and 2E**). We found *NLRP3*

237 (inflammasome) expression during clade III infection at 24 HPI only. There was no
238 significant differential expression of several fungal immune response orthologues, such
239 as *IL-17*, for infection with any clade. Together, these findings suggest that heat shock
240 proteins, nutritional immunity, and the complement effector system are important
241 elements of the AK larval response to *C. auris* microinjection at 37 °C.
242
243 In order to highlight the roles of gene families in the host repsonse, we annotated
244 the AK transcriptome and identified enriched GO terms, KEGG pathways and PFAM
245 domains. Most significantly enriched gene features were identified from responses to
246 infection with the more virulent clades (I and IV) at 48 HPI (**Fig. S2**). The highest mean
247 log-fold changes for any enriched gene features were for clade IV infection, with haem
248 catabolism, haem binding, and haem oxygenase (*HMOX*) related GO terms, KEGG
249 pathway and PFAM domains. Two host orthologues of *HMOX* drove most of these
250 enrichments, such as haem oxidation (log-fold change $\bar{x}$ = 3.96, FDR < 0.0003, **Fig.**
251 **2E**). In terms of other genes involved in iron-nutritional immunity, the AK also up-
252 regulated Ferroxidase Hephaestin (*HPHL1*) in response to clade IV infection, but not
253 Hepcidin (*HEPC1*). The response to clade I infection included 15 enriched GO terms,
254 driven by up-regulation of two orthologues of Laminin subunit-α (*LAMA1*, *LAMA2*, **Fig.**
255 **2D**). No GO terms, KEGG pathways, or PFAM domains were enriched across
256 responses to all five clades. Only one GO term was enriched across responses to four
257 clades, which related to sarcomeric Z-disc in down-regulated genes at 48 HPI (II-V),
258 driven by genes involved in connective and muscular tissue, including *IGFN1* and
259 Calpain-3 (*CAN3*). The response to clade IV infection, in particular, indicates activation
260 of iron metabolism and sequestration, potentially comprising an iron-nutritional immunity
261 response to infection.
262

263 ## *C. auris* xenosiderophore transporter expression was enriched across all five
264 clades during in-host infection
265
266 To identify infection-specific *C. auris* gene expression, we compared the in-host
267 transcriptome to expression induced by growth in a standard rich laboratory media
268 (YPD). Principle components and sample correlation clustering from gene expression
269 data indicated a predominant separate clustering of *in vivo vs in vitro* conditions,
270 indicating that the gene expression profile of *C. auris* during infection is substantially
271 different to that when it is grown in nutrient-rich laboratory media (**Fig. S1G and S1H**).
272 Using the clade I reference genome to align transcripts, we identified 960 DEGs
273 between *in vivo* AK infection at 24 HPI or 48 HPI *versus in vitro* culture in YPD over
274 24 h (499 up-regulated, 523 down-regulated, 17.7% of potential genes, **Fig. 3A**). We
275 identified few DEGs between the two time-points 24 HPI to 48 HPI, with zero DEGs for
276 clade IV and V (**Fig. 3B**). Numbers of up-regulated DEGs unique to any single set were
277 highest for individual clades, particularly in the filamentous clade V at 24 HPI and in the
278 more virulent clades I and IV at 48 HPI (**Fig. 3C-D**). Additionally, we aligned transcripts
279 to clade-specific reference genomes and performed functional annotation and
280 enrichment to identify key biological processes employed across all five clades. Six GO
281 terms, KEGG terms or PFAM domains were enriched across in-host all five clades at
282 48 HPI, related to major facilitator superfamily carbohydrate and siderophore-iron
283 transmembrane transport (**Fig. S4**). This highlighted the expected importance of up-
284 regulation of genes involved in sugar uptake *in vivo vs in vitro*, but also raised the
285 unexpected possibility that up-regulation of members of the *C. auris* expanded gene
286 family of siderophore transporters could be a general feature of in-host infection.
287
288 To describe a core signature of *in vivo* gene expression across the species, we
289 identified the set of 31 DEGs that were significant for all five clades of *C. auris* when
290 transcripts were aligned to the clade I reference (**Fig. 3E, Table S3**). Thirteen DEGs
291 common to all clades of in-host transcription were transmembrane transporters,
292 including up-regulation of transporters for xenosiderophores (*SIT1_3921*, *SIT1_1487*),

293 sugar (*HGT2*, *HGT12*), ammonia (*ATO2*), and nicotinic acid (*TNA1*), and down-
294 regulated drug-resistance-related efflux pumps (*MDR2* and *DTR1*) and peptide
295 transporters (*TPO3*, *PTR22*). Several putative virulence factors such as lipase *LIP1* and
296 cell wall-related *KRE6* and *SOD6* were also down-regulated across all five clades. We
297 demonstrated prominent DEGs (such as down-regulated *ALS4* and *MDR1*) that were
298 significant for at least one clade by mean log-fold change expression volcano plots (**Fig.**
299 **3F**). We also noted that several members of the *SIT1* family were differentially
300 expressed by at least one clade, but were not significant across all five clades, including
301 five genes that were significantly up-regulated across four clades (*SIT1_1542*,
302 *SIT1_1457*, *SIT1_1458*, *SIT1_2110*, and *SIT1_4097*) and five that were up-regulated in
303 one (*SIT1_0002* and *SIT1_2465*), two (*SIT1_3908* and *SIT1_2465*) or three clades
304 (*SIT1_2241*). Two more family members were down-regulated across three clades
305 (*SIT1_1519* and *SIT1_1499*). To nuance these findings further, we noted that two up-
306 regulated genes were also down-regulated in one (*SIT1_3908*) or two clades
307 (*SIT1_2465*). The many up-regulated members of the *SIT1* expanded gene family
308 highlighted the potential importance of the wider family for in-host survival.
309
310 To examine orthologues across reference genomes for each clade (**Fig. S3**), we
311 identified 5,324 orthogroups across clades I-V with outliers *C. haemulonii* and
312 *C. albicans* containing 95.4% of all genes (*n* = 38,345 genes, **Fig. S3A-B**). The use of
313 clade-specific reference genomes identified higher numbers of DEGs (692 *vs* 499 up-
314 regulated and 714 *vs* 523 down-regulated genes) including genes within the accessory
315 genome (55 *vs* 40 up-regulated and 57 *vs* 45 down-regulated, **Fig. S3C**), which we
316 defined as orthogroups of genes not found in every clade. The core genome across all
317 three species and five clades of *C. auris* included 3619 single copy orthologues
318 ($\bar{x}$ = 66.9% *C. auris* genome per clade) and a further 869 single copy orthologues in
319 *C. auris* ($\bar{x}$ = 82.9% *C. auris* genome per clade), of which 133 were unique to *C. auris*.
320 The remaining core genome included 486-585 multiple copy orthologues shared across
321 all species and 110-121 in *C. auris*, of which 17-19 were present in each clade
322 ($\bar{x}$ = 643.2 genes per clade), bringing the total estimated core genome size to

323 5131.2/5413.2 genes per clade ($\bar{x}$ = 94.8%). A single copy orthologue tree confirmed
324 the basal status of clade V, and synteny plotting was consistent with limited
325 transversions/inversions within *C. auris* outwith clade II **Fig. S3A**. These findings are
326 consistent with a highly conserved core yeast genome across *Candida* species,
327 especially within the *Metschinikowiaceae* clade, which appears to contain a degree of
328 preserved genome structure.
329
330 We observed high correlation between log-fold change values obtained from
331 clade-specific and core (B8441) reference genomes (Pearson's >= 0.95, p <0.001 per
332 comparison). Among DEGs that had no orthologues in the clade I reference genome
333 (**Fig. S3D**), the highest number of clade-unique genes that were differentially expressed
334 was identified in clade IV; other DEGs included genes involved in cell wall, intracellular
335 transport, metabolism, transcription/translation and transmembrane transport (**Table**
336 **S3**). In terms of siderophore transporters, we additionally identified a clade IV unique
337 gene associated with a siderophore transport GO term that was differentially expressed
338 at both time-points of infection (CJJ09_005327). Overall, the *in vivo* expression profile
339 across five *C. auris* clades indicated a potential role for the expanded gene family of
340 siderophore transporters during *C. auris* in-host survival and pathogenicity, which was
341 up-regulated compared to growth in nutrient-rich laboratory media.
342
343 **More virulent *C. auris* clades I and IV up-regulated the non-mating *MTL* gene,**
344 ***PIKA*, and down-regulated *MDR1***
345
346 Given significant differences in virulence between clades, we examined gene
347 expression differences between clades I and IV (more virulent) and II and III (less
348 virulent), excluding clade V due to its major morphological differences. Using the clade I
349 reference genome, we identified 623 up-regulated and 779 down-regulated DEGs
350 expressed in clades I and IV, of which 14 were up-regulated and 22 were down-
351 regulated across all comparisons. In order to explore potential drivers of virulence, we
352 excluded DEGs that were significant only for *in vitro* comparisons and examined the

353 remaining set of 10 DEGs shared across all *in vivo* comparisons (I *vs* II, I *vs* III, IV *vs* II,
354 IV *vs* III, **Fig. 4A**, **Table S3**). Strikingly, three of these genes were non-mating genes
355 located at the mating-type locus (*MTL*), including poly-A polymerase *PAP1*, oxysterol
356 binding protein *OBPA* and phosphatidylinositol 4-kinase *PIKA* (**Fig. 4B**). Within the set
357 of 10 DEGs shared across all comparisons, several genes outside the *MTL* were up-
358 regulated, including vacuolar protein sorting gene, *VPS70*, and filamentous growth
359 regulator, *FGR14*. Additionally, the drug efflux pump, *MDR1*, was down-regulated
360 across all comparisons, supporting the idea of a fitness trade-off between resistance
361 and virulence.
362
363 Notably, clades I and IV contain the **a**-type *MTL*, whereas clades II, IV and V
364 contain the **α**-type *MTL*. That both *MTL* contain the non-mating genes is a conserved
365 feature across *Candida* species, in which the *MTL**a*** and *MTL**α*** genes occupy alternative
366 positions. Comparing transcript levels across *MTL* genes in all five clades, we observed
367 poorer detection of *MTL**α*** transcripts when aligned to the clade I reference genome, as
368 expected (**Fig. S5A**). Direct transcript-level testing, with correction for multiple testing to
369 minimise false positives, indicated that only up-regulation of *PIKA* and *PGA30* (48 HPI)
370 and down-regulation of *THI4* (24 HPI) and *MDR1* (at both time-points) were significantly
371 different across the set of 10 DEGs shared across all comparisons (**Fig. S5B**).
372
373 We used the clade I reference genome to annotate functional domains and
374 discover enriched gene families, revealing enrichment of up-regulated hypha-regulated
375 cell wall GPI-anchored proteins in more virulent clades (**Fig. S4**), driven by three pairs
376 of orthologues of *IFF4*, *HYR3* and *RBR3* (**Table S3**). Four secretory lipase *LIP1*
377 paralogues drove an enrichment of the related PFAM domain for clade I *vs* III at 24 HPI.
378 When comparing clade I and IV infection to clade II and 48 HPI, we also observed up-
379 regulated nutrient transporters including a 7 transmembrane domain putative ferric
380 reductase/iron importer, *CFL4*, as well as ferric reductase, *FRE3*, and siderophore
381 transporter orthologues *SIT1_1948*, *SIT1_2241* and *SIT1_4097*. Cell wall components,
382 non-mating *MTL* locus genes such as *PIKA*, and genes involved in iron and siderophore

383 transport are therefore potential modulators of strain-specific differences in virulence.
384
385 **Typical and atypical hypha formation programmes in basal clade V during AK**
386 **yolk-sac infection**
387
388 To explore drivers of filamentation by the clade V strain, we identified 1,046
389 DEGs between clade V and each of the other clades (I-IV), comprising 601 up-regulated
390 and 526 down-regulated genes across all comparisons when using the claded I
391 reference genome. We then identified a set of 57 genes shared across all comparisons
392 for *in vivo* conditions only, since we did observe filamentation in nutrient-rich YPD. 22
393 genes were up-regulated at 24 HPI, 7 at 48 HPI, and 18 at both time-points (**Fig. 4C**).
394 The majority of up-regulated genes were metabolic (*n* = 13), including two cytochrome
395 P450 *ERG5* orthologues, though *ERG11* was down-regulated. Transmembrane
396 transporters for sugar (including two *HGT13* orthologues), amino acids and
397 siderophores (*SIT1_1487*) were also up-regulated (*n* = 10). Cell wall genes up-regulated
398 in filamentous clade V (*n* = 8) included the novel adhesin *SCF1*, GPI-anchored genes
399 *PGA31* and *IFF4*, and orthologues of classical *C. albicans* hyphal adhesins *ALS3* and
400 *RBR3*. We identified differentially expressed transcription factors and related regulators,
401 such as *HAP41* and the pheromone receptor *STE2*, which could play a governing role
402 on these responses. Given the minor differences in numbers of DEGs identified when
403 using clade-specific reference genomes, we also compared the transcript levels for
404 each gene in this set with annotations to identify a highly strict shortlist of inter-clade
405 difference. Using this method, the only significant differences were for up-regulation of
406 *MED7* and *SPS19* (at 24 HPI) and two *HGT13* orthologues and *RNH70* (at both time-
407 points, **Fig. S6**).
408
409 We also examined significant DEGs between clade V and at least one other
410 clade using mean-log fold change (**Fig. 4D**). Several genes that play critical roles in
411 *C. albicans* hypha formation were highly up-regulated, such as transcription factor
412 *UME6* and hypha-specific G1 cyclin-dependent protein serine/threonine kinase *HGC1*.

413 Enrichment analysis indicated up-regulated gene sets involving CFEM domain,
414 cytochrome P450/oxidoreductase activity, hypha-regulated cell wall GPI-anchored
415 proteins and siderophore transport, particularly at 24 HPI and comparing clade V to
416 clade II (**Fig. 4D**). Significantly up-regulated iron-related transport genes in clade V
417 included *FRE3*, *CFL4*, *FRP1*, *SIT1_1519*, *SIT1_1487*, *SIT1_4097*, *SIT1_1542*, and
418 *SIT1_1499*. These findings are consistent with the preservation of a major filamentation
419 programme in *C. auris*, demonstrated in the basal clade V, with unique characteristics
420 such as expression of *SCF1* and the up-regulation of several members of the expanded
421 family of siderophore transmembrane transporters.
422

423 **Xenosiderophore transporters are a *Metschnikowiaceae*-specific expanded gene**
424 **family with varied expression patterns in *C. auris* infection**
425

426 Given the prominence of *SIT1* orthologues across the transcriptomic analyses of
427 *C. auris* during *in vivo* gene expression, we set out to characterise the expanded gene
428 family across orthogroups, including outgroup species *C. haemulonii* and *C. albicans*.
429 **Fig. 5A** shows the predicted structure of *Sit1_1542* (AlphaFold 3). Blastp searches
430 identified proteins with sequence similarity across seven orthologue clusters, of which
431 two main groupings of transporters with 14 transmembrane domains (TMRs) emerged
432 (**Fig. 5B**). A larger branch was annotated with GO term, KEGG pathway and PFAM
433 domains relating to siderophore import (including 12 genes in clade I), and a smaller
434 branch was annotated with GO terms relating to haem transmembrane import (including
435 5 genes in clade I). The majority of orthologues retained 14 TMRs, and few had
436 evidence of additional annotations except for the trichothecene mycotoxin efflux pump
437 PFAM domain across multiple groupings. The orthologue *SIT1_1547* contained 12
438 TMRs and was up-regulated with *SIT1_1548* containing 2 TMRs, which was not
439 identified as a *SIT1* orthologue in our pipeline but has previously been described as
440 such[31,84].
441

442 Co-expression analysis, using simple unweighted Pearson's correlation approach
443 with a cut-off of 0.85, demonstrated eight clusters featuring *SIT1* orthologues, one of
444 which included five that were co-expressed (**Fig. 5C**). To understand how our *in vivo*
445 expression of *C. auris* compared to other experimental conditions previously reported,
446 we measured gene expression across publicly available RNA-seq datasets, identifying
447 35 datasets for which we were able to ascertain gene expression using our pipeline, but
448 none of which included an in-host setting (**Table S4**). Gene expression patterns within
449 the set of single copy orthologues clustered within both principal components analysis
450 of experimental unit variance (**Fig. S3E**) and hierarchical clustering of $\log_{10}$ variance per
451 gene (**Fig. 3F**). We used this data to examine unweighted Pearson's correlation co-
452 expression as above for *SIT1* orthologues among single copy orthologue genes,
453 identifying two clusters only, featuring *SIT1_2110* and *SIT1_1519* (**Fig. 5D**). Given the
454 difference in co-expression patterns between the responses identified in the AK marine
455 host across this study, and a broader meta-analysis of available RNA-seq data, these
456 results highlight a potentially unique influence of a marine larval host environment on
457 transcription programmes and the need to explore in-host time series data with robust
458 weighted co-expression networks in the future.
459
460 To explore the evolutionary history of *SIT1*-related genes in fungi, we performed
461 Blastp searches for orthologues of *C. albicans SIT1* using an e-value cut-off of $1e^{-20}$
462 across 226 fungal species' reference genomes totalling 304 genomes. Separately, 28
463 *Oomycota* genomes were found to contain zero orthologues. We identified 1,689 hits,
464 which clustered into two branches: a smaller branch (n = 397) annotated for siderophore
465 transport including the 12 *C. auris* groupings which we have designated
466 "xenosiderophore transporter candidates" (*XTC*), and a larger branch (n = 1,292)
467 featuring genes predicted (by GO term) to encode haem transporters, including the 5
468 *C. auris* groupings, which we have additionally designated "haem transport-related"
469 (*HTR*, **Fig. 6A**). There were no putative haem transporters or members of the larger
470 branch for *C. albicans*, which only contained the single *SIT1* gene. We calculated the
471 mean number of orthogroups per genome per species (**Fig. 6B**). This showed the most

472 prominent expansion of the *XTC* branch in the *Metschnikowiaceae* clade, including
473 *C. auris* (12 orthologues) and even more so in *C. haemulonii*, with 15 orthologues. No
474 other fungal species or group of species contained so many. *XTC* orthologues were not
475 present in any members of the basal blasocladiomycota, chytridiomycota and
476 mucoromycota, or in several ascomycota (e.g. *Pichia kudriavzevii*,
477 *Schizosaccharomyces pombe* and *Pyricularia oryzae*) and basidiomycota (e.g. *Ustilago*
478 *maydis*). Common human fungal pathogens such as *Aspergillus fumigatus*, *C. albicans*
479 and *Nakaseomyces glabratus* contained only one *XTC* orthologue (**Fig. 6B**). The *HTR*
480 clade, by contrast, was more prominent across fungal phyla, with as many as nine in
481 *Mucor* species, 16 in *A. flavus* and 22 in *F. solani*. We therefore propose a naming of
482 these two expanded gene families as *XTC1-12* and *HTR1-5* in *C. auris*.
483
484 We note the absence of *XTC5* in clade V, *XTC10* in clade IV, and in addition to
485 these, *XTC4*, *XTC9* and *XTC11* in clade II (**Fig. 6C**). Interestingly, clade II, which
486 exhibits the greatest degree of *XTC* gene loss, is also considered to be the least virulent
487 strain. It is also noteworthy that the AK embryo expressed *HMOX* genes during clade IV
488 infection, while clade IV *C. auris* up-regulated *HTR1*, *HTR2* and *HTR5*. This suggests a
489 specific host-pathogen interaction axis in nutritional immunity related to haem
490 scavenging. No other clades of infection were associated with such iron-related
491 functional enrichment in the host, and no other clades expressed more than one *HTR*
492 gene (except *HTR1* and *HTR5* in clade III at 48 HPI). Clade II down-regulated *HTR1* in-
493 host. In summary, *XTC1*, *XTC2*, *XTC3*, *XTC4*, *XTC6*, *XTC7*, *XTC11* and *XTC12* were
494 up-regulated while *XTC8*, *XTC9* and *XTC12* were down-regulated *in vivo* in at least one
495 clade, while up-regulation of *XTC3* and *XTC7* was significant across all clades.
496 Additionally, the more virulent clades were associated with up-regulation of *XTC4*,
497 *XTC5*, and *XTC8*. The filamentous clade V up-regulated *XTC7* across comparisons with
498 all other clades, and up-regulated *XTC1*, *XTC4*, *XTC8* and *XTC9* compared to at least
499 one other clade.
500

501 ## Discussion

502

503 We have described a model for comparative functional genomics of *C. auris* in-
504 host survival using AK yolk-sac microinjections at a clinically relevant temperature in
505 living tissue of a host featuring mammalian-relevant innate immunity. All five clades
506 demonstrated lethality, with a increase in virulence during clades I and IV infection,
507 consistent with clinical and laboratory findings[29]. In-host growth was similar across all
508 clades and high enough to indicate a large enough *in vivo* fungal burden for robust bulk
509 transcriptome interrogation across the species. The contained nature of the yolk-sac
510 provides a host tissue growth medium that enables the assessment of pathogen
511 survival and virulence strategies *in vivo* and a straightforward experimental unit of host
512 tissue without the challenges of pathogen RNA isolation such as locating foci of
513 infection in larger animals. Additional time-points at could be an informative future area
514 of study to develop fine-resolution strain-specific transcription networks. Furthermore,
515 the potential of a transclucent and genetically tractable fish embryo model could enable
516 future visualisation of cellular dynamics and genetic pathway manipulation[77]. Thus, an
517 AK yolk-sac microinjection model has the potential to fill a substantial need for *in vivo*
518 gene expression studies in general.

519

520 We investigated the host transcriptional response to *C. auris* infection, which
521 featured an innate immune response, as expected. The most highly up-regulated gene
522 family included two heme oxygenase (*HMOX*) genes. *HMOX* genes have been shown
523 to mask iron from invading pathogens as a feature of anti-*Candida* nutritional
524 immunity[85], so presumably have a similar function against *C. auris*. This was particularly
525 notable given *HMOX* genes were up-regulated in response to clade IV infection, and the
526 clade IV isolate had a corresponding significant up-regulation of 3 haem transport-
527 related *HTR* genes. In addition to nutritional immunity genes, we found up-regulated
528 heat shock and complement cascade genes during infection, confirming the expected
529 immune response to fungal infection[66,67]. Genes with complex roles in immunity were

530 up-regulated, such as *NLRP3*, for which *C. auris* may be less activating than e.g. *C.*
531 *albicans*[27,86]. It is notable that the yolk-sac model was not associated with histological or
532 transcriptional evidence of host neutrophil recruitment and activation, which may relate
533 to the hypothesis that *C. auris* is immunoevasive[34]. Reference genome bias resulting
534 from the available adult gill transcriptome assembly[87] may limit detection of host gene
535 expression features, so future long and short read assembly from gene expression data
536 across a range of larval stages could further understanding of AK immunity.
537
538 We provided a thorough investigation of differential expression by *C. auris* during
539 infection of host tissue compared with *in vitro* conditions for the first time. The lack of a
540 major distinction across time-points (24 *vs* 48 HPI) indicates that the transcriptional
541 activity of *C. auris* in-host was highly similar at these stages. Six functional annotation
542 terms (GO, KEGG pathway and PFAM domain) were significantly enriched among
543 genes that were up-regulated across all five clades, including sugar and siderophore
544 transporters. The enrichment of sugar transporters outside of nutrient-rich YPD-broth is
545 unsurprising, such as High-affinity Glucose Transporter *HGT12*, with evidence of
546 redundancy in *C. albicans*[88–91], and *HGT2*, part of an eight-gene "core filamentation
547 response network" in *C. albicans*[92]. More surprising was the down-regulation of putative
548 virulence factors such as Secreted Aspartyl Protease 3 (*SAP3*), thought to be the most
549 important SAP in *C. auris*, and required for virulence in a mouse model[26], and Copper
550 Superoxide Dismutase *SOD6*, which has been shown to be down-regulated in iron
551 starvation[93]. Multi-drug efflux pumps such as *MDR2* (down-regulated *in vivo*) and *MDR1*
552 (down-regulated *in vivo* and in clades I and IV *vs* clades II and III) are understood to
553 drive drug resistance through multiple but unclear mechanisms in *C. auris*[94,95]; in-host
554 down-regulation may indicate a fitness trade-off for virulence *vs* drug resistance.
555
556 The mating type locus (*MTL*) genes have been hypothesised to contribute to
557 virulence in fungal species including *Cryptococcus neoformans*[96]. Given that *C. auris* is
558 assumed not to undergo meiotic recombination[97], there is a question of what role *MTL*-
559 associated genes play in pathogenicity and morphology. Two of the three non-mating

560 genes (*PAP1* and *PIKA*) in the *MTL* were up-regulated by more virulent strains (I and
561 IV) compared to the less virulent strains (II and III). Importantly, the two more virulent
562 clades (I and IV) contain *MTL**a*** rather than *MTL**α*** (clades II & III)[23], and clades V and VI
563 contain *MTL**a*** and *MTL**α*** respectively[12]. Thus, it is unclear if the up-regulation of non-
564 mating genes is a *MTL* specific transcriptional nuance, or a feature of more highly
565 virulent *C. auris* clades. The *MTL* also did not feature prominently in the filamentation
566 response observed in clade V, providing no evidence for an obvious role for the *MTL* in
567 such morphological changes.
568
569 Filamentation is an important pathogenicity trait in fungi, especially *Candida*
570 species, although its roles have been more poorly described in aquatic infections[98]. We
571 observed *in vivo* filamentation by a representative strain of *C. auris* clade V, the
572 basal/ancestral clade[99], accompanied by a genera-typical filamentous gene expression
573 signature. Specifically, we measured the up-regulation of *HGC1* and *UME6*, which are
574 two of the most important regulators of filamentation in *C. albicans*, and have recently
575 been described as drivers of *C. auris* filamentation and biofilm formation[100]. The
576 expression of adhesin *SCF1* in filamenting clade V is noteworthy because its cationic
577 adhesion mechanism has been postulated to be consistent with adhesion mechanisms
578 common to marine organisms including bivalves[21]. The generalist marine-isolated
579 pathogen *C. haemulonii* has also displayed filamentation competence at lower
580 temperatures[101], consistent with an ancestral aquatic state.
581
582 Human histopathology reports of *C. auris* infection are rarely published and have
583 not demonstrated classical in-host filamentation, to our knowledge. An *ex vivo* human
584 epithelial model using a clade I isolate did demonstrate filamentous *C. auris* at 37 °C
585 after injection into deeper dermis[102]. Clade III *C. auris* has also been observed to form
586 filamentous/hyphal forms in *Galleria mellonella* injection[61]. Fan and colleagues have
587 observed filamentous forms of *C. auris* across all four clades, even demonstrating a
588 higher virulence in the *G. mellonella* model[103], though the phenotype required passage
589 through a murine host with additional prolonged growth at 25 °C for at least 5 days

590 before and after injection[19]. Other stimuli have induced filamentation in clade I isolates,
591 such as hydroxyurea genotoxic stress[104] and Hsp90 inhibition[105], where several up-
592 regulated genes in *C. auris* filamentation (*SCF1*, *IFF4* and *PGA31*) matched those in
593 our study. Constitutive filamentous growth has also been demonstrated with a
594 transposon-mediated disruption of a long non-coding RNA[106], which sit adjacent to
595 chitin deacetylase *CDA2*, which was down-regulated at 24 HPI in this experiment during
596 filamentation. These findings indicate that hyphal formation is possible across *C. auris*
597 clades.
598
599 A total of twelve siderophore transporters were up-regulated during infection, and
600 four were down-regulated, with three family members up-regulated in more virulent
601 clades and five in the filamentous clade V. The fact that siderophore transporter up-
602 regulation has also been detected during *ex vivo* whole blood infection by *C. auris*
603 underscores the likelihood that our findings are clinically relevant[31]. Interestingly, this
604 family of predicted xenosiderophore transporter genes is significantly expanded in
605 several members of the *Metschnikowiaceae* clade compared to other
606 *Saccharomycetae*[23], raising questions as to the roles of siderophore transporters in
607 *C. auris* biology and evolution[107]. Siderophore synthesis may be unlikely in *C. auris*,
608 given the lack of evidence in other *Candida* species[108]. As a result, *C. albicans* Sit1,
609 which is required for virulence[109], is thought to be a xenosiderophore transporter for
610 iron-chelators produced by other microbes and specific to the ferrioxamine type
611 common in iron-poor ocean environments[110,111]. Siderophore transporters can also act
612 intracellularly for compartments such as the mitochondrion[112,113], or act as efflux pumps
613 for various molecules[114] including trichothecene mycotoxins as identified by our
614 functional annotations.
615
616 *C. auris* encodes a large expanded gene family of 17 siderophore transporters
617 that we named xenosiderophore transporter candidates (*XTC*) 1-12 and haem
618 transport-related (*HTR*) genes 1-5, the latter sharing sequence similarity with *S. pombe*
619 low-affinity haem transporter Str3[115]. In other *Candida* species such as *C. albicans*, iron

620 assimilation is understood to be central for in-host survival[116,117], where deprivation
621 triggers various pathogenic programmes such as alterations in cell surface beta-
622 glucan[118]. Haem is acquired by *C. albicans* through vesicular endocytosis and CFEM-
623 domain containing proteins[119,120] and does not contain *HTR* genes, suggesting a
624 possible loss of transmembrane haem transporters. The ubiquity of *HTR* across the
625 fungal kingdom and lack of *XTC* genes in the three basal fungal phyla suggest that
626 *SIT1*/*HTC* could have arisen from a duplication of an *HTR*-related gene in the Dikarya
627 (the ascomycota and basidiomycota) with subsequent independent loss of both *XTC*
628 and *HTC* genes in multiple fungal lineages. Our identification of up-regulated *XTC*
629 transport during infection corroborates the findings of up-regulated *XTC2A-B*
630 (*B9J08_1547-8*) in an *ex vivo* blood model of *C. auris* infection[31]. These findings
631 together suggest the importance of iron during infection, which could be targeted in the
632 clinic, e.g. via low-toxicity pyrvinium pamoate[121].
633
634 We show for the first time an *in vivo* infection host tissue transcriptional profile for
635 the critical priority WHO human fungal pathogen *C. auris*. Representative strains from
636 all five major clades of the recent simultaneous emergences highlighted strain-specific
637 differences in morphology, virulence and gene expression. This study highlights the
638 advantages and potential of a clinically relevant thermotolerant yolk-sac injection model,
639 adding to the debate around the putative marine origins of *C. auris*, and the emergence
640 of distinct clades. We demonstrate natural filamentation by clade V and virulence
641 difference for clades I and IV, and comprehensively describe associated gene
642 expression. We indicate the importance of the *XTC* and *HTR* gene clusters as
643 recommended targets for investigation of fungal biology, pathogenicity and treatment.
644 Our findings shed new light on the emergence and evolution of *C. auris* from a probable
645 marine yeast ancestor. We therefore reveal mechanisms that enable *C. auris* to survive
646 in host tissue and provide a step forward in understanding the pathobiology of an
647 emerging fungal pathogen and global public health threat.
648

649 ## Methods

650

651 **Ethical Statement:** All animal experiments were performed under Project
652 Licence PP4402521 in compliance with University of Exeter Animal Welfare Ethical
653 Review Board regulations and MRC Center for Medical Mycology Project Review
654 Board, and are reported in line with "Animal Research: Reporting *in vivo* Experiments"
655 (ARRIVE 2.0) Guidelines[122].

656

657 ***Aphanius dispar* Care, Monitoring, Husbandry and Procedures:** Wild-type
658 adult AK were kept at the Aquatic Resources Facility, Exeter, in two 28 °C incubation
659 tanks, with 12-hour day and night light cycles and artificial enrichment foliage. Embryos
660 were collected using three plastic netted collection chambers per tank with transfer of all
661 enrichment into tanks, and placed overnight from 16:00 to 09:15 in dark conditions.
662 Chambers were then drained, cleaned and strained with 35 parts per thousand artificial
663 seawater (ASW) to isolate all embryos. Subsequent ASW was sterile suction filtered *via*
664 0.2 µm pore Nalgene Rapid-Flow (Thermo Scientific, UK). Embryos were inspected for
665 viability in terms of an intact blastocyst without discolouration by stereo dissection
666 microscope (Optech, UK) and incubated at 30 °C (Memmert, Germany) for 72 h with
667 day and night cycles with daily ASW changes and removal of dead, unhealthy or
668 underdeveloped embryos, with a maximum of 30 embryos per standard size 100 mm x
669 15 mm petri dish (Greiner Bio-One, Austria). Excluded embryos were killed or disposed
670 of either by submission in Virkon solution (Sigma-Aldrich, UK) or freezing at -80 °C.

671

672 **Experimental Procedures:** Injection needles were prepared using borosilicate
673 glass capillaries (Harvard apparatus, USA) and a heated pulling system (heater level >
674 62, PC-10, Narishige, UK). We used tweezers to snap the tip to an estimated 1 mm
675 graticule-measured aperture of 10-20 µm, and sterilised needles before use with
676 253.7 nm UV light over 15 minutes (Environmental Validation Solutions, UK). Injection
677 bays were made with microwaved 1% agarose in 1 g (Sigma, USA) per 100 mL ASW

678 for up to 24 embryos in 100 mm petri dishes using custom-made molds in an inverted
679 60 mm petri dish. Embryos were randomly chosen from each dish and the sequence of
680 injection for each biological repeat was randomly allocated by computer. For
681 microinjection, *C. auris* yeasts were counted by haemocytometer and added to 25 µL
682 sterile filtered phenol red solution 0.5% (Sigma, UK) to a concentration of $0.5x10^8$ per
683 mL in 100 µL. Injection needles were loaded with 5 µL injection solution using 20 µL
684 Microloader EpT.I.P.S. (Eppendorf, UK) immediately before injection of up to 30
685 embryos before re-loading. Injections were performed with 400-500 hPa injection
686 pressure and 7-40 hPa compensation pressure over 100-200 ms with the FemtoJet 4i
687 (Eppendorf UK) using a micromanipulator (World Precision Instruments, UK) and a
688 Microtec HM-3 stereo dissection microscope (Optech, UK). In order to deliver a dose of
689 approx. 500 yeasts in 10 nL solution, an injection bolus was administered to an
690 estimated diameter of 0.2 – 0.3 mm (10-15% of total embryo diameter) *via* a single
691 chorion puncture. Any embryos that failed to meet these criteria for injection were
692 excluded. Control *in vitro* inoculations were microinjected as above into 1 mL YPD in
693 1.5 mL Eppendorf tubes before incubation without shaking at 37 °C for 24 h
694 contemporaneously with embryos as below.
695
696 **Study Design and Sample Sizes:** We used an unblinded prospective virulence
697 study comparing six groups of AK embryo yolk-sac microinjection, including five
698 different clades of *C. auris*, and one control sham injection as the negative control. We
699 used >= 23 embryos per condition based on our power calculation of σ = 0.25,
700 significance = 0.05, power = 0.9, and δ effect size of 25% mortality (two-sided t-test).
701 After excluding embryos that were unhealthy or did not complete successful
702 microinjection, we included *n* = 10-13 embryos per group per experiment (total *n* = 34-
703 37 embryos per group). Each embryo was considered to be an experimental unit
704 (*n* = 70-72 embryos per experiment, total *n* = 213 embryos). For estimation of *C. auris*
705 in-host growth by homogenisation and plating of colony forming units, three embryos
706 per condition per time-point across two (0 and 24 HPI) or three (48 HPI) experiments
707 were used (total *n* = 126). For time lapse microscopy demonstration of *A. dispar* yolk-

708 sac collapse and death, representative image sets were chosen from a pilot experiment
709 using a reduced dosage (1/10) of *C. auris* (*n* = 4). For histological demonstration of
710 *C. auris* morphology, one embryo per condition at 24 HPI and 48 HPI each were used in
711 one experiment, and seven embryos per condition plus three embryos without injection
712 in a second experiment (*n* = 57). RNA was extracted from three embryos per condition
713 per time-point (0, 24 and 48 HPI, *n* = 54) plus three embryos per time-point without any
714 injection (*n* = 9, total *n* = 63) as a control for the impact of microinjection.
715
716 ***C. auris* Strains and Growth:** We selected five *C. auris* strains to represent
717 each major clade (**Table S1**). Culture stocks were kept in -80 °C in Yeast extract
718 Peptone Dextrose (YPD) broth (Sigma-Aldrich, UK) containing 25% glycerol
719 (ThermoFisher, UK) and plated onto YPD-agar (Sigma-Aldrich) for 48 h before
720 innoculation and overnight growth in 10 mL YPD broth at 30 °C in a shaking incubator at
721 200 rpm (Multitron, Infors HT, UK). Five mL from each overnight culture was then
722 centrifuged at 5000 g for 2 minutes before triple washing in 1 mL autoclaved deionised
723 water (DIW, Milli-Q, Merck, USA) to prevent aggregation[22], then re-suspended again in
724 200 µL DIW. Decontamination of surfaces was conducted with both mopping and
725 cleaning wipes in 70% Ethanol (Sigma-Aldrich) or 10% Chemgene HLD_4L (Medimark
726 Scientific, UK) as per manufacturer's instructions. For growth curves, *C. auris* strains
727 were grown overnight in YPD in 4 replicates. Overnight cultures were inoculated into
728 YPD to a final OD 600 of 0.02 in a 96-well plate. OD was read over 25 hourly cycles at
729 37 °C with 300 s shaking at 2.5 mm amplitude on an Infinite 200 PRO plate reader
730 (Tecan, Switzerland).
731
732 **Outcome measurement:** individual embryos were kept in 1 mL sterile filtered
733 ASW per embryo in a 48 well flat bottom plate (Corning, USA) sealed with Parafilm "M"
734 (Bemis Company, USA) at 37 °C with passive humidification using a 500 mL open glass
735 beaker of water. Embryos were monitored for presence of heart rate at 24-hourly
736 intervals up to 7 days by stereo dissection microscope. Initial time of injection was
737 subtracted from each time-point to minimise bias between groups. Kaplan-Meier

738 survival curves were plotted with Log-Rank testing and Benjamini-Hochberg (BH)
739 correction[123] using survival v.3.5.8 and survminer v.0.4.9 packages in R v.4.4.0. Colony
740 forming units (CFUs) were calculated by homogenisation of embryos at 0, 24, and
741 48 HPI by autoclaved plastic micropestle in a 1.5 mL conical tube (Eppendorf, UK) in
742 100 µL 10,000 U/mL penicillin/streptomycin (P/S) solution (Gibco, UK). Dilutions were
743 made with P/S solution and DIW in 1/10-10,000 and counts were adjusted according to
744 dilution after plating onto YPD agar plates and read after 72 h incubation at 30 °C.
745 Statistical testing between CFU numbers was performed with Wilcoxon testing and BH
746 correction.
747
748 **Imaging:** For direct microscopy, AK were kept in 300 µL ASW containing 0.04%
749 Tricaine anaesthesia (Sigma-Aldrich, UK) in an optical adhesive and parafilm-sealed
750 96-well plate. These were then monitored for heart beat by 5 bright field 2X or 4X
751 images at pre-focused z slices taken every 2 h by Acquifer microscopy (Bruker,
752 Germany) over 72 h. All images were processed in ImageJ 1.53a (NIH, USA).
753 Sectioning and staining was performed by Microtechnical Services, Exeter, UK, with
754 fixation of embryos in 1 mL 10% neutral-buffered formalin (Sigma-Aldrich, UK) for >
755 24 h, followed by immersion in 4% phenol 10 mL glycerine BP made up to 100 mL with
756 distilled water[124], sectioned at 4 µm without orientation, and stained with Harris
757 Haematoxylin & 1% Alcoholic Eosin on Leica Autostainer. H&E stained histological
758 sections were imaged on an Olympus IX83 microscope coupled with an Olympus DP23
759 colour camera using an Olympus UPlanXApo x40/0.95 objective controlled by cellSens
760 software v.3.2. Brightfield microscopy was performed with an EVOS M5000 microscope
761 (ThermoFisher, UK). Microscopy of YPD-agar grown colonies was performed without
762 staining in DIW.
763
764 **RNA Extraction and Sequencing:** Total RNA was extracted using the
765 Monarch® Total RNA Miniprep Kit (NEB, USA). Embryos were flash frozen in liquid
766 nitrogen, re-suspended in DNA/RNA Protection Reagent and disrupted with an
767 autoclaved plastic micropestle. Bead beating was performed in a FastPrep 24

768 homogeniser (MP Biomedicals) with 0.5 mm zirconia/silica beads for 8 cycles of 35 s at
769 6 m/s plus 45 s on ice. Lysate was recovered and incubated for 5 min. at 55 °C with
770 proteinase K before addition of lysis buffer and RNA purification following
771 manufacturer's instructions. Total RNA samples were quantified using the Qubit 4.0
772 Fluorometer (Invitrogen, USA) and integrity was checked with the Tapestation 4200
773 (Agilent, USA). Library preparation and sequencing were performed by the Exeter
774 Sequencing Service. Samples were normalised and prepared using the NEBNext Ultra
775 II Directional RNA Library Prep - Poly(A) mRNA Magnetic Isolation Module following the
776 standard protocol. Libraries were sequenced on a Novaseq 6000 sequencer with 150bp
777 paired-end reads. Reads were trimmed with fastp[125] v.0.23.1 to remove reads < 75
778 bases and trim based from the 3' end with q-score < 22. Quality control was performed
779 with FastQC (https://github.com/s-andrews/FastQC) v.0.11.9 and MultiQC[126] v.1.6.
780
781 **Differential Gene Expression:** We aligned sequences ($\bar{x}$ = 52.9 m reads per
782 replicate, range 41.1-112.2 m) using the Trinity pipeline[127] v.2.15.1 to the *C. auris* clade
783 I B8441 reference genome (GCA_002759435.2)[23] downloaded from GenBank (mean
784 aligned reads in infected embryos 3.83 m, 0.81-13.1%). We further aligned clade-
785 specific reference genomes for each strain (**Table S1**), including clade II
786 (GCA_003013715.2)[4], III (GCA_002775015.1)[13], IV (GCA_008275145.1)[13] and V
787 (GCA_016809505.1)[99,128,129]. We aligned conditions containing *A. dispar* to the *de novo*
788 GJEY01 adult gill transcriptome assembly[87] downloaded from GenBank, for which we
789 detected expression over 27,481 potential genes. Alignment was performed with
790 Bowtie2[130] v.2.5.1, transcript estimation with RNA Seq by Expectation Maximisation
791 (RSEM)[131] v.1.3.3, differential expression with EdgeR[132] v.3.40.0, Samtools[133] v.1.17
792 and limma[134] v.3.54.0 using a false discovery rate (FDR) p-value cut-off of 0.001 and a
793 log fold change cut-off of +/-2.0. Principal components were calculated and plotted
794 using the prcomp function in Rv4.4.0 and ggfortify v.0.4.17 R package for fragments per
795 kilobase per million, and correlations plots from counts per million as per the default
796 output of the Trinity pipeline. Log fold change was plotted with ComplexHeatmap[135].
797

798 **Annotation and Enrichment:** Gene ontology terms[136,137] were assigned using
799 DIAMOND[138] v.2.1.8 *via* the DIAMOND2GO pipeline[139] for each of the *C. auris*
800 reference genomes. KEGG terms[140] were assigned using the BlastKOALA online
801 platform using the eukaryote database[141]. Protein FAMily (PFAM) domains[142] were
802 identified using the PFAM-A.hmm database
803 (https://ftp.ebi.ac.uk/pub/databases/Pfam/current_release/Pfam-A.full.gz) and HMMER
804 and HMM Scan[143] with a cut-off of $1e^{-5}$. Further domain-specific identification was
805 performed with SignalP 5.0[144], DeepTMHMM 1.0[145] and NetGPI 1.1[146]. Enrichment
806 analysis for DEG subsets was calculated using the Fisher's Exact test, adjusted using
807 the Benjamini-Hochberg method per set of up-regulated or down-regulated features in
808 each comparison as a conservative estimate of significant gene set enrichment, with a
809 false discovery rate cutoff of p=0.001. Annotation tables were checked with additional
810 information from available literature, supplemented by details and web-scraped
811 orthologue names from *Candida* Genome Database[84] and Blastp searches[147].
812 Annotations for the GJEY01 genome were also performed using Diamond2GO,
813 BlastKoala and HMMScan as above and checked against *A. dispar* annotations and
814 gene names obtained directly from the GJEY01 transcriptome makers[87]. For plotting,
815 lists of GO terms were identified (and for *A. dispar* enrichment, reduced by removal of
816 redundant terms) by REVIGO[148].
817
818 **Orthologue Assignment:** To identify accessory genes across *C. auris* clades,
819 we used the Synima pipeline[149] with Orthofinder v2.5.5[150] with additional reference
820 genomes for *C. albicans* (SC5314_GCA_000182965.3) and *C. haemulonii*
821 (B11899_ASM1933202v1). We also incorporated a very recent version of the *C. auris*
822 B8441 assembly (v3) to arrange contigs and illustrate re-arrangements, with broad
823 syntenic concordance; it contains 5 more genes than v2, for which 27 (0.5%) and 16
824 (0.3%) genes were unique to each genome, respectively. Multiple alignment of single
825 copy orthologues as defined by Orthofinder was performed with Muscle v5.1[151] and a
826 phylogeny was made with FastTree v2.1.11[152] using default settings.
827

828 **RNA-Seq Meta-Analysis Variance:** NCBI SRA was searched for
829 "*Candida auris*" on 16th April 2024 and downloaded as metadata *via* the "Send to: Run
830 Selector" function. Each project accession number for runs containing RNA was
831 searched against available published literature to identify publications, noting subject of
832 study, clades/strains, growth media, comparative conditions, temperature and time
833 scales used. Calculation of FPKM was performed and analysed as above using the set
834 of single copy orthologues to demonstrate variance via PCA with ggfortify and prcomp
835 packages in R and to calculate an unweighted co-expression Pearson's correlation (cut-
836 off of 0.85) for *SIT1* genes with and without the additional data from the RNA-Seq meta-
837 analysis.
838
839 ***SIT1* Analysis:** The protein transcript for *C. albicans SIT1* was Blastp searched
840 against the draft pangenome database as above. We visualised the structure using
841 Alphafold v3[153] and ChimeraX v1.8[154]. Clade I-V *C. auris* and *C. haemulonii SIT1* genes
842 were aligned using Muscle as above before using RAXML-NG v1.2.2 with 1000
843 bootstraps and the LG4X model[155], which was visualised using ggtree v3.12.0 and
844 gheatmap. For panfungal *SIT1* analysis, we used the fungidb portal for Blastp using the
845 *C. albicans SIT1* against all available fungal data (with no hits within oomyceta),
846 including 274 reference genomes representing 197 species and a cut-off of $1e^{-20}$.
847 Annotations for each protein transcript were performed as above to obtain GO terms,
848 KEGG pathways, PFAM domains, GPI-anchors, SignalP domains, and transmembrane
849 domains, while a phylogeny for *SIT1* similar sequences across all fungal references was
850 constructed as above following multiple alignment with Clustal Omega v1.2.4[156]
851
852 **Data Availability:** Raw reads have been deposited via NCBI/GEO *via* accession
853 GSE277854. All datasets and code required to make figures are available via Github
854 (https://github.com/hughgifford/Arabian_Killifish_C_auris_2024).
855

856 ## References

857

858 1. Meis, J. F. & Chowdhary, A. *Candida auris*: A global fungal public health threat.
859 *The Lancet Infectious Diseases* **18**, 1298–1299 (2018).

860 2. WHO. World Health Organisation (WHO) fungal priority pathogens list to guide
861 research, development and public health action. (2022)
862 doi:https://www.who.int/publications/i/item/9789240060241.

863 3. Lee, W. G. *et al.* First three reported cases of nosocomial fungemia caused by
864 *Candida auris*. *Journal of Clinical Microbiology* **49**, 4 (2011).

865 4. Satoh, K. *et al.* *Candida auris* sp. Nov., a novel ascomycetous yeast isolated
866 from the external ear canal of an inpatient in a Japanese hospital. *Microbiology and*
867 *Immunology* **53**, 41–44 (2009).

868 5. Lyman, M. Notes from the field: Transmission of pan-resistant and echinocandin-
869 resistant *Candida auris* in health care facilities - Texas and the District of Columbia,
870 January-April 2021. *Morbidity and Mortality Weekly Report* **70**, (2021).

871 6. Eyre, D. W. *et al.* A *Candida auris* outbreak and its control in an intensive care
872 setting. *New England Journal of Medicine* **379**, 1322–1331 (2018).

873 7. Taori, S. K. *et al.* *Candida auris* outbreak: Mortality, interventions and cost of
874 sustaining control. *Journal of Infection* **79**, 601–611 (2019).

875 8. Shuping, L. *et al.* High prevalence of *Candida auris* colonization during protracted
876 neonatal unit outbreak, South Africa. *Emerging Infectious Diseases* (2023)
877 doi:10.3201/eid2909.230393.

878 9. Adam, R. D. *et al.* Analysis of *Candida auris* fungemia at a single facility in
879 Kenya. *International Journal of Infectious Diseases* **85**, 182–187 (2019).

880 10. Prayag, P. S., Patwardhan, S., Panchakshari, S., Rajhans, P. A. & Prayag, A.
881 The dominance of *Candida auris*: A single-center experience of 79 episodes of

882 candidemia from western India. *Indian Journal of Critical Care Medicine* **26**, 560–563
883 (2022).

884 11. Khan, T. *et al.* Emergence of the novel sixth *Candida auris* clade VI in
885 Bangladesh. *Microbiology Spectrum* **12**, e03540–23 (2024).

886 12. Suphavilai, C. *et al.* Detection and characterisation of a sixth *Candida auris* clade
887 in Singapore: A genomic and phenotypic study. *Lancet Microbe* **0**, (2024).

888 13. Lockhart, S. R. *et al.* Simultaneous emergence of multidrug-resistant *Candida*
889 *auris* on 3 continents confirmed by whole-genome sequencing and epidemiological
890 analyses. *Clinical Infectious Diseases* **64**, 134–140 (2017).

891 14. Gifford, H., Rhodes, J. & Farrer, R. A. The diverse genomes of *Candida auris*.
892 *The Lancet Microbe* **0**, (2024).

893 15. Chen, J. *et al.* Is the superbug fungus really so scary? A systematic review and
894 meta-analysis of global epidemiology and mortality of *Candida auris*. *BMC Infectious*
895 *Diseases* **20**, 827 (2020).

896 16. Mayer, F. L., Wilson, D. & Hube, B. *Candida albicans* pathogenicity mechanisms.
897 *Virulence* **4**, 119–128 (2013).

898 17. Phan, Q. T. *et al.* Als3 is a *Candida albicans* invasin that binds to cadherins and
899 induces endocytosis by host cells. *PLOS Biology* **5**, e64 (2007).

900 18. Moyes, D. L. *et al.* Candidalysin is a fungal peptide toxin critical for mucosal
901 infection. *Nature* **532**, 64–68 (2016).

902 19. Yue, H. *et al.* Filamentation in *Candida auris*, an emerging fungal pathogen of
903 humans: Passage through the mammalian body induces a heritable phenotypic switch.
904 *Emerging Microbes & Infections* **7**, 1–13 (2018).

905 20. Chadwick, C., Jesus, M. D., Ginty, F. & Martinez, J. S. Pathobiology of *Candida*
906 *auris* infection analyzed by multiplexed imaging and single cell analysis. *PLOS ONE* **19**,
907 e0293011 (2024).

908 21. Santana, D. J. *et al.* A *Candida auris*-specific adhesin, Scf1, governs surface
909 association, colonization, and virulence. *Science* **381**, 1461–1467 (2023).

910 22. Pelletier, C., Shaw, S., Alsayegh, S., Brown, A. J. P. & Lorenz, A. *Candida auris*
911 undergoes adhesin-dependent and -independent cellular aggregation. *PLOS Pathogens*
912 **20**, e1012076 (2024).

913 23. Muñoz, J. F. *et al.* Genomic insights into multidrug-resistance, mating and
914 virulence in *Candida auris* and related emerging species. *Nature Communications* **9**,
915 5346 (2018).

916 24. Richardson, J. P. *et al.* Candidalysins are a new family of cytolytic fungal peptide
917 toxins. *mBio* **13**, e03510–21 (2022).

918 25. Horton, M. V. *et al.* *Candida auris* cell wall mannosylation contributes to
919 neutrophil evasion through pathways divergent from *Candida albicans* and *Candida*
920 *glabrata*. *mSphere* **6**, e00406–21 (2021).

921 26. Kim, J.-S., Lee, K.-T. & Bahn, Y.-S. Secreted aspartyl protease 3 regulated by
922 the Ras/cAMP/PKA pathway promotes the virulence of *Candida auris*. *Frontiers in*
923 *Cellular and Infection Microbiology* **13**, 1257897 (2023).

924 27. Weerasinghe, H. *et al.* *Candida auris* uses metabolic strategies to escape and kill
925 macrophages while avoiding robust activation of the NLRP3 inflammasome response.
926 *Cell Reports* **42**, 112522 (2023).

927 28. Byun, S. A. *et al.* Virulence traits and azole resistance in Korean *Candida auris*
928 Isolates. *Journal of Fungi* **9**, 979 (2023).

929 29. Santana, D. J., Zhao, G. & O'Meara, T. R. The many faces of *Candida auris*:
930 Phenotypic and strain variation in an emerging pathogen. *PLOS Pathogens* **20**,
931 e1012011 (2024).

932 30. Wang, T. W. *et al.* Functional redundancy in *Candida auris* cell surface adhesins
933 crucial for cell-cell interaction and aggregation. *Nature Communications* **15**, 9212
934 (2024).

935 31. Allert, S. *et al.* From environmental adaptation to host survival: Attributes that
936 mediate pathogenicity of *Candida auris*. *Virulence* **13**, 191–214 (2022).

937 32. Fayed, B. *et al.* Transcriptome analysis of human dermal cells infected with
938 *Candida auris* identified unique pathogenesis/defensive mechanisms particularly
939 ferroptosis. *Mycopathologia* **189**, 65 (2024).

940 33. Yang, B. *et al.* A correlative study of the genomic underpinning of virulence traits
941 and drug tolerance of *Candida auris*. *Infection and Immunity* **0**, e00103–24 (2024).

942 34. Balakumar, A. *et al.* Single-cell transcriptomics unveils skin cell specific
943 antifungal immune responses and IL-1Ra- IL-1R immune evasion strategies of
944 emerging fungal pathogen *Candida auris*. *PLOS Pathogens* **20**, e1012699 (2024).

945 35. Bruno, M. *et al.* Transcriptional and functional insights into the host immune
946 response against the emerging fungal pathogen *Candida auris*. *Nature Microbiology* **5**,
947 1516–1531 (2020).

948 36. Wang, Y. *et al.* Innate immune responses against the fungal pathogen *Candida*
949 *auris*. *Nature Communications* **13**, 3553 (2022).

950 37. Wang, X. *et al.* The first isolate of *Candida auris* in China: Clinical and biological
951 aspects. *Emerging Microbes & Infections* **7**, 1–9 (2018).

952 38. Fan, S., Li, C., Bing, J., Huang, G. & Du, H. Discovery of the diploid form of the
953 emerging fungal pathogen *Candida auris*. *ACS Infectious Diseases* **6**, 2641–2646
954 (2020).

955 39. Fan, S. *et al.* A biological and genomic comparison of a drug-resistant and a
956 drug-susceptible strain of *Candida auris* isolated from Beijing, China. *Virulence* **12**,
957 1388–1399 (2021).

958 40. Wurster, S., Albert, N. D. & Kontoyiannis, D. P. *Candida auris* bloodstream
959 infection induces upregulation of the PD-1/PD-L1 immune checkpoint pathway in an
960 immunocompetent mouse model. *mSphere* **7**, e00817–21 (2022).

961 41. Bing, J. *et al.* Rapid evolution of an adaptive multicellular morphology of *Candida*
962 *auris* during systemic infection. *Nature Communications* **15**, 2381 (2024).

963 42. Ben-Ami, R. *et al.* Multidrug-resistant *Candida haemulonii* and *C. auris*, Tel Aviv,
964 Israel. *Emerging Infectious Diseases* **23**, (2017).

965 43. Hager, C. L., Larkin, E. L., Long, L. A. & Ghannoum, M. A. Evaluation of the
966 efficacy of rezafungin, a novel echinocandin, in the treatment of disseminated *Candida*
967 *auris* infection using an immunocompromised mouse model. *Journal of Antimicrobial*
968 *Chemotherapy* **73**, 2085–2088 (2018).

969 44. Zhao, M. *et al.* *In Vivo* Pharmacokinetics and pharmacodynamics of APX001
970 against *Candida* spp. In a neutropenic disseminated candidiasis mouse model.
971 *Antimicrobial Agents and Chemotherapy* **62**, e02542–17 (2018).

972 45. Singh, S. *et al.* The NDV-3A vaccine protects mice from multidrug resistant
973 *Candida auris* infection. *PLOS Pathogens* **15**, e1007460 (2019).

974 46. Zhang, F. *et al.* A marine microbiome antifungal targets urgent-threat drug-
975 resistant fungi. *Science* **370**, 974–978 (2020).

976 47. Muñoz, J. E. *et al.* Pathogenicity levels of Colombian strains of *Candida auris*
977 and Brazilian strains of *Candida haemulonii* species complex in both murine and*Galleria*
978 *mellonella* experimental models. *Journal of Fungi* **6**, 104 (2020).

979 48. Abe, M. *et al.* Potency of gastrointestinal colonization and virulence of *Candida*
980 *auris* in a murine endogenous candidiasis. *PLoS One* **15**, e0243223 (2020).

981 49. Forgács, L. *et al.* Comparison of in vivo pathogenicity of four *Candida auris*
982 clades in a neutropenic bloodstream infection murine model. *Emerging Microbes &*
983 *Infections* **9**, 1160–1169 (2020).

984 50. Nagy, F. *et al.* In vitro and in vivo interaction of caspofungin with isavuconazole
985 against *Candida auris* planktonic cells and biofilms. *Medical Mycology* **59**, 1015–1023
986 (2021).

987 51. Forgács, L. *et al.* In vivo efficacy of amphotericin B against four *Candida auris*
988 Clades. *Journal of Fungi (Basel, Switzerland)* **8**, 499 (2022).

989 52. Singh, S. *et al.* Protective efficacy of anti-Hyr1p monoclonal antibody against
990 systemic candidiasis due to multi-drug-resistant *Candida auris*. *Journal of Fungi* **9**, 103
991 (2023).

992 53. Salama, E. A. *et al.* Lansoprazole interferes with fungal respiration and acts
993 synergistically with amphotericin B against multidrug-resistant *Candida auris*. *Emerging*
994 *Microbes & Infections* **13**, 2322649 (2024).

995 54. Torres, S. R. *et al.* Impact of *Candida auris* infection in a neutropenic murine
996 model. *Antimicrobial Agents and Chemotherapy* **64**, e01625–19 (2020).

997 55. Xin, H., Mohiuddin, F., Tran, J., Adams, A. & Eberle, K. Experimental mouse
998 models of disseminated *Candida auris* infection. *mSphere* **4**, e00339–19 (2019).

999 56. Rosario-Colon, J., Eberle, K., Adams, A., Courville, E. & Xin, H. *Candida* cell-
1000 surface-specific monoclonal antibodies protect mice against *Candida auris* invasive
1001 infection. *International Journal of Molecular Sciences* **22**, 6162 (2021).

1002 57. Torres, S. R. *et al.* Assessment of environmental and occupational exposure
1003 while working with multidrug resistant (MDR) fungus *Candida auris* in an animal facility.
1004 *Journal of Occupational and Environmental Hygiene* **16**, 507–518 (2019).

1005 58. Borman, A. M. Of mice and men and larvae: *Galleria mellonella* to model the
1006 early host-pathogen interactions after fungal infection. *Virulence* **9**, 9–12 (2017).

1007 59. Romera, D. *et al.* The *Galleria mellonella* infection model as a system to
1008 investigate the virulence of *Candida auris* strains. *Pathogens and Disease* **78**, ftaa067
1009 (2020).

1010 60. García-Carnero, L. C. *et al.* Early virulence predictors during the *Candida*
1011 species–*Galleria mellonella* interaction. *Journal of Fungi* **6**, 152 (2020).

1012 61. Garcia-Bustos, V. *et al.* Characterization of the differential pathogenicity of
1013 *Candida auris* in a *Galleria mellonella* infection model. *Microbiology Spectrum* **9**,
1014 e00013–21 (2021).

1015 62. Carvajal, S. K. *et al.* Pathogenicity assessment of Colombian strains of *Candida*
1016 *auris* in the *Galleria mellonella* invertebrate model. *Journal of Fungi* **7**, 401 (2021).

1017 63. Hernando-Ortiz, A. *et al.* Virulence of *Candida auris* from different clinical origins
1018 in *Caenorhabditis elegans* and *Galleria mellonella* host models. *Virulence* **12**, 1063–
1019 1075 (2021).

1020 64. Spettel, K. *et al.* *Candida auris* in Austria—what is new and what is different.
1021 *Journal of Fungi* **9**, 129 (2023).

1022 65. Wurster, S. *et al.* *Drosophila melanogaster* as a model to study virulence and
1023 azole treatment of the emerging pathogen *Candida auris*. *Journal of Antimicrobial*
1024 *Chemotherapy* **74**, 1904–1910 (2019).

1025 66. Harpf, V., Rambach, G., Würzner, R., Lass-Flörl, C. & Speth, C. *Candida* and
1026 complement: New aspects in an old battle. *Frontiers in Immunology* **11**, 1471 (2020).

1027 67. Pechacek, J. & Lionakis, M. S. Host defense mechanisms against *Candida auris*.
1028 *Expert Review of Anti-infective Therapy* **21**, 1087–1096 (2023).

1029 68. Bavia, L., Santiesteban-Lores, L. E., Carneiro, M. C. & Prodocimo, M. M.
1030 Advances in the complement system of a teleost fish, *Oreochromis niloticus*. *Fish &*
1031 *Shellfish Immunology* **123**, 61–74 (2022).

1032 69. Buchmann, K., Karami, A. M. & Duan, Y. The early ontogenetic development of
1033 immune cells and organs in teleosts. *Fish & Shellfish Immunology* **146**, 109371 (2024).

1034 70. Tian, H. *et al.* Cytokine networks provide sufficient evidence for the differentiation
1035 of CD4+ T cells in teleost fish. *Developmental & Comparative Immunology* **141**, 104627
1036 (2023).

1037 71. Johnson, C. J., Davis, J. M., Huttenlocher, A., Kernien, J. F. & Nett, J. E.
1038 Emerging fungal pathogen *Candida auris* evades neutrophil attack. *mBio* **9**, e01403–18
1039 (2018).

1040 72. Pharkjaksu, S., Boonmee, N., Mitrpant, C. & Ngamskulrungroj, P.
1041 Immunopathogenesis of emerging *Candida auris* and *Candida haemulonii* strains.
1042 *Journal of Fungi* **7**, 725 (2021).

1043 73. Shapiro, R. S. & Cowen, L. E. Uncovering cellular circuitry controlling
1044 temperature-dependent fungal morphogenesis. *Virulence* **3**, 400–404 (2012).

1045 74. Leach, M. D. *et al.* Hsf1 and Hsp90 orchestrate temperature-dependent global
1046 transcriptional remodelling and chromatin architecture in *Candida albicans*. *Nature*
1047 *Communications* **7**, 11704 (2016).

1048 75. Xiao, W. *et al.* Response and regulatory mechanisms of heat resistance in
1049 pathogenic fungi. *Applied Microbiology and Biotechnology* **106**, 5415–5431 (2022).

1050 76. Akbarzadeh, A. & Leder, E. H. Acclimation of killifish to thermal extremes of hot
1051 spring: Transcription of gonadal and liver heat shock genes. *Comparative Biochemistry*
1052 *and Physiology Part A: Molecular & Integrative Physiology* **191**, 89–97 (2016).

1053 77. Hamied, A. *et al.* Identification and characterization of highly fluorescent pigment
1054 cells in embryos of the Arabian killifish (*Aphanius Dispar*). *iScience* **23**, 101674 (2020).

1055 78. Alsakran, A. *et al.* Stage-by-stage exploration of normal embryonic development
1056 in the Arabian killifish, *Aphanius dispar*. *Developmental Dynamics* **n/a**, (2024).

1057 79. Minhas, R. *et al.* The thermotolerant Arabian killifish, *Aphanius dispar*, as a novel
1058 infection model for human fungal pathogens. 2024.10.08.617174 (2024)
1059 doi:10.1101/2024.10.08.617174.

1060 80. Arora, P. *et al.* Environmental isolation of *Candida auris* from the coastal
1061 wetlands of Andaman Islands, India. *mBio* **12**, e03181–20 (2021).

1062 81. Escandón, P. Novel environmental niches for *Candida auris*: Isolation from a
1063 coastal habitat in Colombia. *Journal of Fungi* **8**, 748 (2022).

1064 82. Uden, V. & Kolipinski, M. C. *Torulopsis haemulonii nov. spec.*, A yeast from the
1065 Atlantic Ocean. *Antonie Van Leeuwenhoek* **28**, 78–80 (1962).

1066 83. Burden, N., Chapman, K., Sewell, F. & Robinson, V. Pioneering better science
1067 through the 3Rs: An introduction to the national centre for the replacement, refinement,
1068 and reduction of animals in research (NC3Rs). *Journal of the American Association for*
1069 *Laboratory Animal Science* **54**, 198–208 (2015).

1070 84. Skrzypek, M. S. *et al.* The Candida Genome Database (CGD): Incorporation of
1071 Assembly 22, systematic identifiers and visualization of high throughput sequencing
1072 data. *Nucleic Acids Research* **45**, D592–D596 (2017).

1073 85. Potrykus, J. *et al.* Fungal iron availability during deep seated candidiasis is
1074 defined by a complex interplay involving systemic and local events. *PLOS pathogens* **9**,
1075 e1003676 (2013).

1076 86. Kasper, L. *et al.* The fungal peptide toxin Candidalysin activates the NLRP3
1077 inflammasome and causes cytolysis in mononuclear phagocytes. *Nature*
1078 *Communications* **9**, 4260 (2018).

1079 87. Bonzi, L. C. *et al.* The time course of molecular acclimation to seawater in a
1080 euryhaline fish. *Scientific Reports* **11**, 18127 (2021).

1081 88. Varma, A. *et al.* Molecular cloning and functional characterisation of a glucose
1082 transporter, CaHGT1, of Candida albicans. *FEMS microbiology letters* **182**, 15–21
1083 (2000).

1084 89. Luo, L., Tong, X. & Farley, P. C. The *Candida albicans* gene HGT12
1085 (Orf19.7094) encodes a hexose transporter. *FEMS Immunology & Medical Microbiology*
1086 **51**, 14–17 (2007).

1087 90. Brown, V., Sexton, J. A. & Johnston, M. A glucose sensor in Candida albicans.
1088 *Eukaryotic Cell* **5**, 1726–1737 (2006).

1089 91. Larcombe, D. E. *et al.* Glucose-enhanced oxidative stress resistance-A protective
1090 anticipatory response that enhances the fitness of *Candida albicans* during systemic
1091 infection. *PLOS Pathogens* **19**, e1011505 (2023).

1092 92. Martin, R. *et al.* A core filamentation response network in *Candida albicans* is
1093 restricted to eight genes. *PLOS ONE* **8**, e58613 (2013).

1094 93. Schatzman, S. S. *et al.* Copper-only superoxide dismutase enzymes and iron
1095 starvation stress in Candida fungal pathogens. *The Journal of Biological Chemistry* **295**,
1096 570–583 (2020).

1097 94. Rybak, J. M. *et al.* Abrogation of Triazole Resistance upon Deletion of *CDR1* in a
1098 Clinical Isolate of *Candida auris*. *Antimicrobial Agents and Chemotherapy* **63**, (2019).

1099 95. Li, J., Coste, A. T., Bachmann, D., Sanglard, D. & Lamoth, F. Deciphering the
1100 Mrr1/Mdr1 pathway in azole resistance of *Candida auris*. *Antimicrobial Agents and*
1101 *Chemotherapy* **66**, e00067–22 (2022).

1102 96. Sun, S., Coelho, M. A., David-Palma, M., Priest, S. J. & Heitman, J. The
1103 evolution of sexual reproduction and the Mating-type locus: Links to pathogenesis of
1104 *Cryptococcus* human pathogenic fungi. *Annual Review of Genetics* **53**, 417–444 (2019).

1105 97. Wang, Y. & Xu, J. Population genomic analyses reveal evidence for limited
1106 recombination in the superbug *Candida auris* in nature. *Computational and Structural*
1107 *Biotechnology Journal* **20**, 3030–3040 (2022).

1108 98. Overy, D. P., Rämä, T., Oosterhuis, R., Walker, A. K. & Pang, K.-L. The
1109 neglected marine fungi, *Sensu stricto*, and their isolation for natural products' discovery.
1110 *Marine Drugs* **17**, 42 (2019).

1111 99. Chow, N. A. *et al.* Potential fifth clade of *Candida auris,* Iran, 2018. *Emerging*
1112 *Infectious Diseases* **25**, 1780–1781 (2019).

1113 100. Louvet, M. *et al.* Ume6-dependent pathways of morphogenesis and biofilm
1114 formation in *Candida auris*. *Microbiology Spectrum* **0**, e01531–24 (2024).

1115 101. Deng, Y., Li, S., Bing, J., Liao, W. & Tao, L. Phenotypic switching and
1116 filamentation in *Candida haemulonii*, an emerging opportunistic pathogen of humans.
1117 *Microbiology Spectrum* **9**, e00779–21 (2021).

1118 102. Seiser, S. *et al.* Native human and mouse skin infection models to study *Candida*
1119 *auris*-host interactions. *Microbes and Infection* **26**, 105234 (2024).

1120 103. Fan, S. *et al.* Filamentous growth is a general feature of *Candida auris* clinical
1121 isolates. *Medical Mycology* **59**, 734–740 (2021).

1122 104. Bravo Ruiz, G., Ross, Z. K., Gow, N. A. R. & Lorenz, A. Pseudohyphal growth of
1123 the emerging pathogen *Candida auris* is triggered by genotoxic stress through the S
1124 phase checkpoint. *mSphere* **5**, e00151–20 (2020).

1125 105. Kim, S. H. *et al.* Genetic analysis of *Candida auris* implicates Hsp90 in
1126 morphogenesis and azole tolerance and Cdr1 in Azole Resistance. *mBio* **10**, e02529–
1127 18 (2019).

1128 106. Gao, J. *et al.* LncRNA DINOR is a virulence factor and global regulator of stress
1129 responses in *Candida auris*. *Nature Microbiology* **6**, 842–851 (2021).

1130 107. Chybowska, A. D., Childers, D. S. & Farrer, R. A. Nine things genomics can tell
1131 us about *Candida auris*. *Frontiers in Genetics* **11**, 351 (2020).

1132 108. Ismail, A., Bedell, G. W. & Lupan, D. M. Siderophore production by the
1133 pathogenic yeast, *Candida albicans*. *Biochemical and Biophysical Research*
1134 *Communications* **130**, 885–891 (1985).

1135 109. Heymann, P. *et al.* The Siderophore iron transporter of *Candida albicans*
1136 (Sit1p/Arn1p) mediates uptake of ferrichrome-type siderophores and Is required for
1137 epithelial invasion. *Infection and Immunity* **70**, 5246–5255 (2002).

1138 110. Boiteau, R. M. *et al.* Siderophore-based microbial adaptations to iron scarcity
1139 across the eastern Pacific Ocean. *Proceedings of the National Academy of Sciences*
1140 **113**, 14237–14242 (2016).

1141 111. Park, J. *et al.* Siderophore production and utilization by marine bacteria in the
1142 North Pacific Ocean. *Limnology and Oceanography* **68**, 1636–1653 (2023).

1143 112. Renshaw, J. C. *et al.* Fungal siderophores: Structures, functions and
1144 applications. *Mycological Research* **106**, 1123–1142 (2002).

1145 113. Johnstone, T. C. & Nolan, E. M. Beyond iron: Non-classical biological functions
1146 of bacterial siderophores. *Dalton Transactions* **44**, 6320–6339 (2015).

1147 114. Nakajima, Y. *et al.* Effect of disrupting the trichothecene efflux pump encoded by
1148 *FgTri12* in the nivalenol chemotype of *Fusarium graminearum*. *The Journal of General*
1149 *and Applied Microbiology* **61**, 93–96 (2015).

1150 115. Xue, P. *et al.* Heme sensing and trafficking in fungi. *Fungal Biology Reviews* **43**,
1151 100286 (2023).

1152 116. Fourie, R., Kuloyo, O. O., Mochochoko, B. M., Albertyn, J. & Pohl, C. H. Iron at
1153 the Centre of *Candida albicans* Interactions. *Frontiers in Cellular and Infection*
1154 *Microbiology* **8**, 185 (2018).

1155 117. Alselami, A. & Drummond, R. A. How metals fuel fungal virulence, yet promote
1156 anti-fungal immunity. *Disease Models & Mechanisms* **16**, dmm050393 (2023).

1157 118. Pradhan, A. *et al.* Non-canonical signalling mediates changes in fungal cell wall
1158 PAMPs that drive immune evasion. *Nature Communications* **10**, 5315 (2019).

1159 119. Weissman, Z. & Kornitzer, D. A family of *Candida* cell surface haem-binding
1160 proteins involved in haemin and haemoglobin-iron utilization. *Molecular Microbiology* **53**,
1161 1209–1220 (2004).

1162 120. Ding, C. *et al.* Conserved and divergent roles of Bcr1 and CFEM proteins in
1163 *Candida parapsilosis and Candida albicans*. *PLOS ONE* **6**, e28151 (2011).

1164 121. Simm, C. *et al.* Disruption of iron homeostasis and mitochondrial metabolism are
1165 promising targets to inhibit *Candida auris*. *Microbiology Spectrum* **10**, e00100–22
1166 (2022).

1167 122. Sert, N. P. du *et al.* Reporting animal research: Explanation and elaboration for
1168 the ARRIVE guidelines 2.0. *PLOS Biology* **18**, e3000411 (2020).

1169 123. Benjamini, Y. & Hochberg, Y. Controlling the false discovery rate: A practical and
1170 powerful approach to multiple testing. *Journal of the Royal Statistical Society Series B:*
1171 *Statistical Methodology* **57**, 289–300 (1995).

1172 124. Bancroft, J. & Stevens, A. Theory and Practice of Histological Techniques.
1173 (1977).

1174 125. Chen, S., Zhou, Y., Chen, Y. & Gu, J. Fastp: An ultra-fast all-in-one FASTQ
1175 preprocessor. *Bioinformatics* **34**, i884–i890 (2018).

1176 126. Ewels, P., Magnusson, M., Lundin, S. & Käller, M. MultiQC: Summarize analysis
1177 results for multiple tools and samples in a single report. *Bioinformatics* **32**, 3047–3048
1178 (2016).

1179 127. Haas, B. J. *et al.* De novo transcript sequence reconstruction from RNA-seq
1180 using the Trinity platform for reference generation and analysis. *Nature Protocols* **8**,
1181 1494–1512 (2013).

1182 128. Abastabar, M. *et al.* *Candida auris* otomycosis in Iran and review of recent
1183 literature. *Mycoses* **62**, 101–105 (2019).

1184 129. Muñoz, J. F. *et al.* Clade-specific chromosomal rearrangements and loss of
1185 subtelomeric adhesins in *Candida auris*. *Genetics* **218**, iyab029 (2021).

1186 130. Langmead, B. & Salzberg, S. L. Fast gapped-read alignment with Bowtie 2.
1187 *Nature Methods* **9**, 357–359 (2012).

1188 131. Li, B. & Dewey, C. N. RSEM: Accurate transcript quantification from RNA-Seq
1189 data with or without a reference genome. *BMC Bioinformatics* **12**, 323 (2011).

1190 132. Robinson, M. D., McCarthy, D. J. & Smyth, G. K. edgeR: A Bioconductor
1191 package for differential expression analysis of digital gene expression data.
1192 *Bioinformatics* **26**, 139–140 (2010).

1193 133. Li, H. *et al.* The Sequence Alignment/Map format and SAMtools. *Bioinformatics*
1194 **25**, 2078–2079 (2009).

1195 134. Ritchie, M. E. *et al.* Limma powers differential expression analyses for RNA-
1196 sequencing and microarray studies. *Nucleic Acids Research* **43**, e47 (2015).

1197 135. Gu, Z., Eils, R. & Schlesner, M. Complex heatmaps reveal patterns and
1198 correlations in multidimensional genomic data. *Bioinformatics* **32**, 2847–2849 (2016).

1199 136. Ashburner, M. *et al.* Gene Ontology: Tool for the unification of biology. *Nature*
1200 *Genetics* **25**, 25–29 (2000).

1201 137. The Gene Ontology Consortium *et al.* The Gene Ontology knowledgebase in
1202 2023. *Genetics* **224**, iyad031 (2023).

1203 138. Buchfink, B., Reuter, K. & Drost, H.-G. Sensitive protein alignments at tree-of-life
1204 scale using DIAMOND. *Nature Methods* **18**, 366–368 (2021).

1205 139. Golden, C., Studholme, D. J. & Farrer, R. A. DIAMOND2GO: A rapid Gene
1206 Ontology assignment and enrichment tool for functional genomics. 2024.08.19.608700
1207 (2024) doi:10.1101/2024.08.19.608700.

1208 140. Kanehisa, M., Furumichi, M., Sato, Y., Kawashima, M. & Ishiguro-Watanabe, M.
1209 KEGG for taxonomy-based analysis of pathways and genomes. *Nucleic Acids Research*
1210 **51**, D587–D592 (2022).

1211 141. Kanehisa, M., Sato, Y. & Morishima, K. BlastKOALA and GhostKOALA: KEGG
1212 tools for functional characterization of genome and metagenome sequences. *Journal of*
1213 *Molecular Biology* **428**, 726–731 (2016).

1214 142. Bateman, A. *et al.* The Pfam protein families database. *Nucleic Acids Research*
1215 **32**, D138–D141 (2004).

1216 143. Eddy, S. R. Accelerated Profile HMM Searches. *PLOS Computational Biology* **7**,
1217 e1002195 (2011).

1218 144. Almagro Armenteros, J. J. *et al.* SignalP 5.0 improves signal peptide predictions
1219 using deep neural networks. *Nature Biotechnology* **37**, 420–423 (2019).

1220 145. Hallgren, J. *et al.* DeepTMHMM predicts alpha and beta transmembrane proteins
1221 using deep neural networks. (2022) doi:10.1101/2022.04.08.487609.

1222 146. Gíslason, M. H., Nielsen, H., Almagro Armenteros, J. J. & Johansen, A. R.
1223 Prediction of GPI-anchored proteins with pointer neural networks. *Current Research in*
1224 *Biotechnology* **3**, 6–13 (2021).

1225 147. Camacho, C. *et al.* BLAST+: Architecture and applications. *BMC Bioinformatics*
1226 **10**, 421 (2009).

1227 148. Supek, F., Bošnjak, M., Škunca, N. & Šmuc, T. REVIGO summarizes and
1228 visualizes long lists of gene ontology terms. *PLOS ONE* **6**, e21800 (2011).

1229 149. Farrer, R. A. Synima: A Synteny imaging tool for annotated genome assemblies.
1230 *BMC Bioinformatics* **18**, 507 (2017).

1231 150. Emms, D. M. & Kelly, S. OrthoFinder: Phylogenetic orthology inference for
1232 comparative genomics. *Genome Biology* **20**, 238 (2019).

1233 151. Edgar, R. C. MUSCLE: Multiple sequence alignment with high accuracy and high
1234 throughput. *Nucleic Acids Research* **32**, 1792–1797 (2004).

1235 152. Price, M. N., Dehal, P. S. & Arkin, A. P. FastTree 2 – approximately maximum-
1236 likelihood trees for large alignments. *PLOS ONE* **5**, e9490 (2010).

1237 153. Abramson, J. *et al.* Accurate structure prediction of biomolecular interactions with
1238 AlphaFold 3. *Nature* **630**, 493–500 (2024).

1239 154. Pettersen, E. F. *et al.* UCSF ChimeraX: Structure visualization for researchers,
1240 educators, and developers. *Protein Science* **30**, 70–82 (2021).

1241 155. Stamatakis, A. RAxML version 8: A tool for phylogenetic analysis and post-
1242 analysis of large phylogenies. *Bioinformatics* **30**, 1312–1313 (2014).

1243 156. Sievers, F. & Higgins, D. G. Clustal omega. *Current Protocols in Bioinformatics*
1244 **48**, 3.13.1–3.13.16 (2014).

1245 ## End Matter

1246

1247 ### Acknowledgements

1248

1249 We acknowledge funding from the MRC Centre for Medical Mycology at the
1250 University of Exeter (MR/N006364/2, MR/V033417/1), MRC Doctoral Training Grants
1251 MR/P501955/2 and MR/W502649/1, Wellcome Trust (206412/A/17/Z), Wellcome Trust
1252 Career Development Award (215239/Z/19/Z) and Wellcome Trust Fellowship
1253 (219551/Z/19/Z), National Centre for the Replacement, Refinement and Reduction of
1254 Animals in Research (NC3Rs) (NC/X001121/1), and the NIHR Exeter Biomedical
1255 Research Centre. TB also was supported *via* Elizabeth Ballou and a Sir Henry Dale
1256 Fellowship jointly funded by the Wellcome Trust and the Royal Society (211241/Z/18/Z)
1257 and the Lister Institute. The views expressed are those of the authors and not
1258 necessarily those of the NIHR or the Department of Health and Social Care. We thank
1259 staff in the Aquatic Resource Center at the University of Exeter for husbandry of the fish

and the support for developing protocols for feeding, spawning, and raising new generations of this relatively new model species, including Sam Worthington, Chloe Flint and Richard Silcox. We also thank the Exeter Sequencing Service facility and support from Wellcome Trust Institutional Strategic Support Fund (WT097835MF), Wellcome Trust Multi User Equipment Awards (WT101650MA and 218247/Z/19/Z), Medical Research Council Clinical Infrastructure Funding (MR/M008924/1) and BBSRC LOLA award (BB/K003240/1). We also thank the University of Exeter High-Performance Computing (HPC) facility funded by the UK MRC Clinical Research Infrastructure Initiative (award number MR/M008924/1). We thank Tanmoy Chakraborty, Dhara Malavia and Neil Gow for providing *C. auris* strains, Teigan Veale, Sumita Roy, Jonathan Ball and Darren Thomson for assistance in microscopy and Chloe Pelletier for advice on aggregation. We also thank Microtechnical Services, Exeter, UK, for assistance with histological sectioning.

Author Contributions

HG: designed and conducted experiments, performed analysis, drafted and wrote the paper. NH, JG, QM, TB: optimised, designed or performed experiments. RF, TK, TB, MR, JR, DW, AB: designed experiments, obtained funding. All authors edited the manuscript.

Competing Interests

JR has received honoraria from Gilead for conference presentations. Other authors declare no competing interests.

ORCID IDs

HG (https://orcid.org/0000-0003-2797-852X), TB (https://orcid.org/0000-0002-5315-2759), NH (https://orcid.org/0000-0003-0260-023X), JG (https://orcid.org/0009-

0003-3803-9496), QM (https://orcid.org/0000-0001-9892-4997), AB (https://orcid.org/0000-0002-7381-131X), DW (https://orcid.org/0000-0001-6617-0123), JR (https://orcid.org/0000-0002-1338-7860), MR (https://orcid.org/0009-0009-0746-4127), TK (https://orcid.org/0000-0002-5373-2737), RF (https://orcid.org/0000-0001-8456-7458)

Figures

```
Warning: package 'magick' was built under R version 4.4.1

Warning: package 'lubridate' was built under R version 4.4.1
```

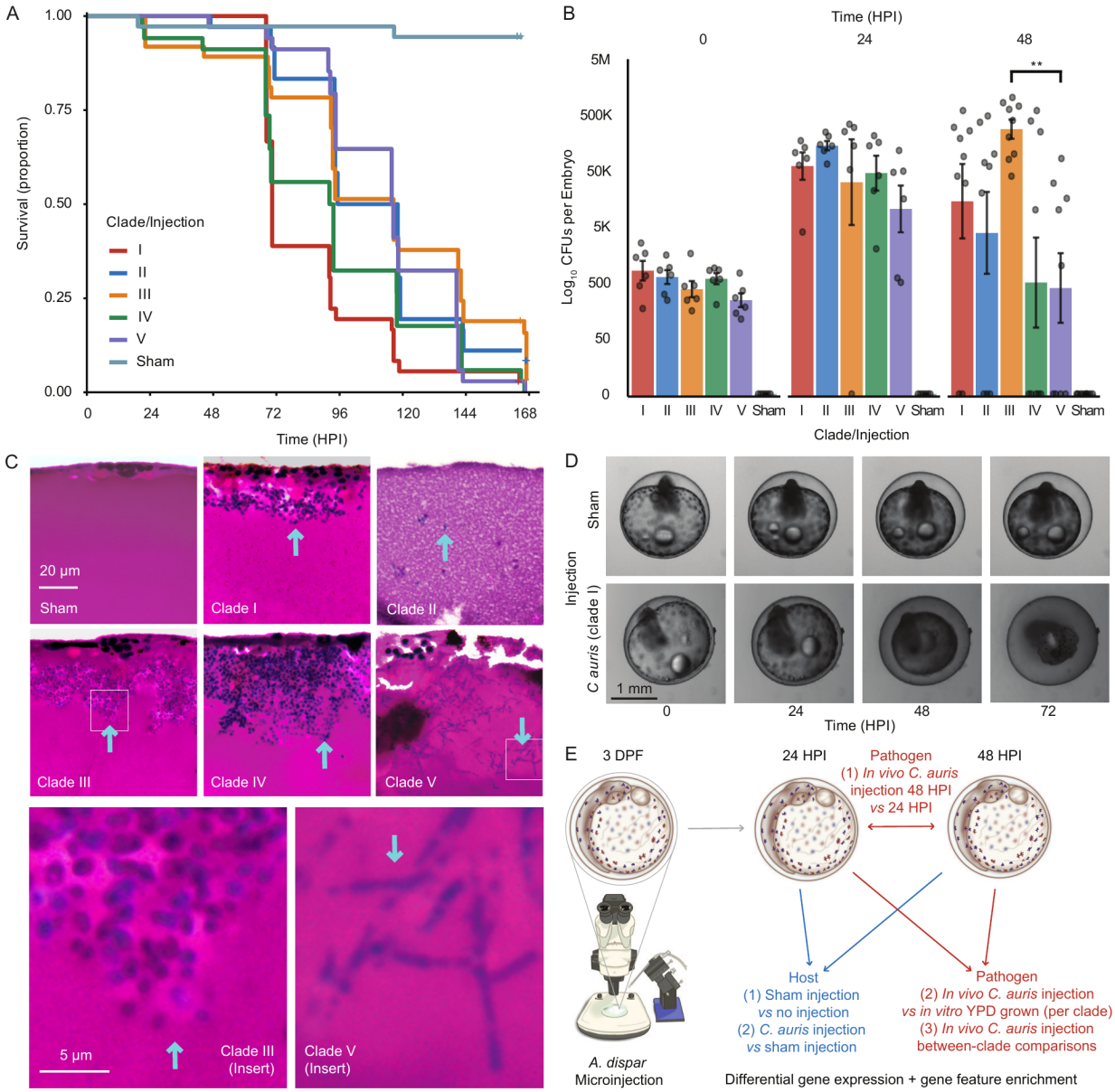

Figure 1. Modelling *C. auris* infection in the Arabian killifish (A) Survival curves for embryos injected with each *C. auris* clade or sham injection. Significance testing between groups is given in **Table S1**; hours post injection (HPI). **(B)** Colony forming units (CFUs) per clade from embryos homogenised after injection as an indicator of injection dose and *in vivo* growth. **(C)** H&E Staining of AK yolk-sac at 48 HPI for each clade or sham injection; morphology is indicated by blue arrows, with insets indicating

1307 typical yeast (clade III) and filamentous morphology (clade V). The yolk-sac edge is
1308 oriented at the top. **(D)** Illustrative time-lapse microscopy of embryo death including
1309 yolk-sac collapse during infection (clade I infection) or survival (sham injection) using
1310 Acquifer live imaging. **(E)** Experimental scheme for differential gene expression analysis
1311 of RNA extracted from AK embryos injected at 3 days post fertilisation (DPF).

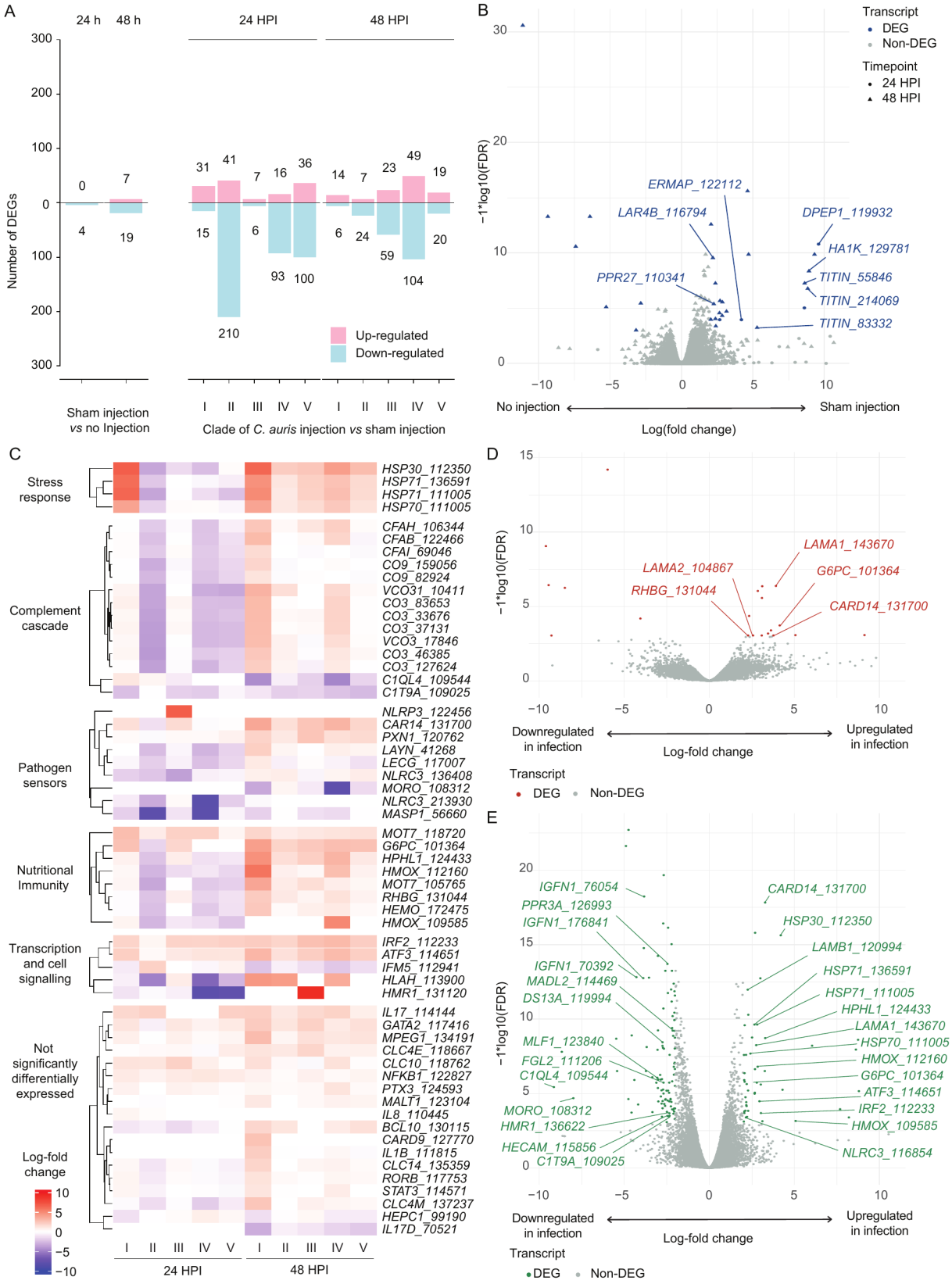
A
24 h
48 h
24 HPI
48 HPI
Number of DEGs
Up-regulated
Down-regulated
Sham injection vs no Injection
Clade of C. auris injection vs sham injection
B
Transcript
DEG
Non-DEG
Timepoint
24 HPI
48 HPI
−1*log10(FDR)
ERMAP_122112
LAR4B_116794
DPEP1_119932
HA1K_129781
PPR27_110341
TITIN_55846
TITIN_214069
TITIN_83332
No injection
Sham injection
Log(fold change)
C
Stress response
Complement cascade
Pathogen sensors
Nutritional Immunity
Transcription and cell signalling
Not significantly differentially expressed
Log-fold change
24 HPI
48 HPI
D
LAMA1_143670
LAMA2_104867
G6PC_101364
RHBG_131044
CARD14_131700
Downregulated in infection
Upregulated in infection
Log-fold change
Transcript
DEG
Non-DEG
E
IGFN1_76054
CARD14_131700
PPR3A_126993
HSP30_112350
IGFN1_176841
LAMB1_120994
IGFN1_70392
HSP71_136591
MADL2_114469
HSP71_111005
DS13A_119994
HPHL1_124433
LAMA1_143670
MLF1_123840
HSP70_111005
FGL2_111206
HMOX_112160
C1QL4_109544
G6PC_101364
ATF3_114651
MORO_108312
IRF2_112233
HMR1_136622
HMOX_109585
HECAM_115856
NLRC3_116854
C1T9A_109025
Downregulated in infection
Upregulated in infection
Log-fold change
Transcript
DEG
Non-DEG

1312

1313 **Figure 2. AK host responses to *C. auris* infection: (A)** Number of differentially
1314 expressed genes (DEGs) for each of two comparisons, sham injection *vs* no injection
1315 (left panel), and *C. auris* injection *vs* sham injection (right panel), at either 24 or 48 h
1316 post injection (HPI). **(B)** Volcano plot showing log-fold change and significance
1317 according to -$\log^{10}$ false discovery rate (FDR) for sham injection *vs* no injection. **(C)**
1318 Heatmap demonstrating log-fold change for differential expression between *C. auris*
1319 injection and sham injection for groups of genes. **(D-E)** Volcano plots showing log-fold
1320 change and significance for DEGs expressed during infection with the two more virulent
1321 clades of *C. auris* at 48 HPI, clade I (**D**, DEGs in red) and clade IV (**E**, DEGs in green).

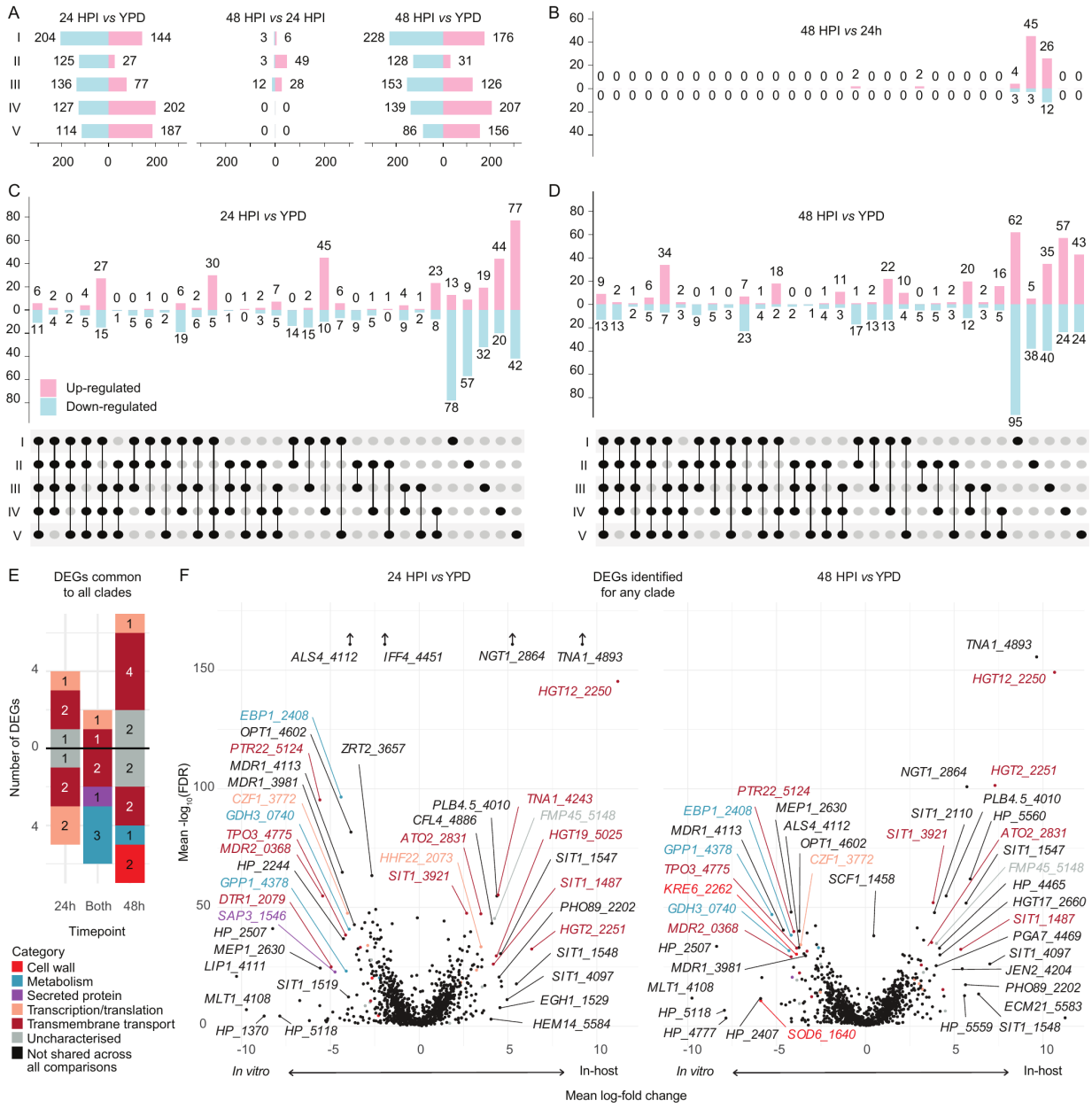

Figure 3: *C. auris* gene expression *in vivo vs in vitro* (A) Total DEGs per clade for each comparison between 24 h post injection (HPI), 48 HPI, and growth in YPD alone. **(B-D)** Upset plots for each comparison, indicating DEGs that were significant across all five clades (far left) and for each individual clade (far right) and each set in between. **(E)** Combined set of significant DEGs common to all five clades between *in vivo* infection and *in vivo* growth in YPD. Genes are coloured by manually annotated category (**Table**

S4). **(F)** Volcano plots demonstrate mean log-fold change for DEGs identified for any clade. Genes with infinite false discovery rate (FDR) are indicated with an arrow. Genes included in the combined set are coloured by category as per panel **E**.

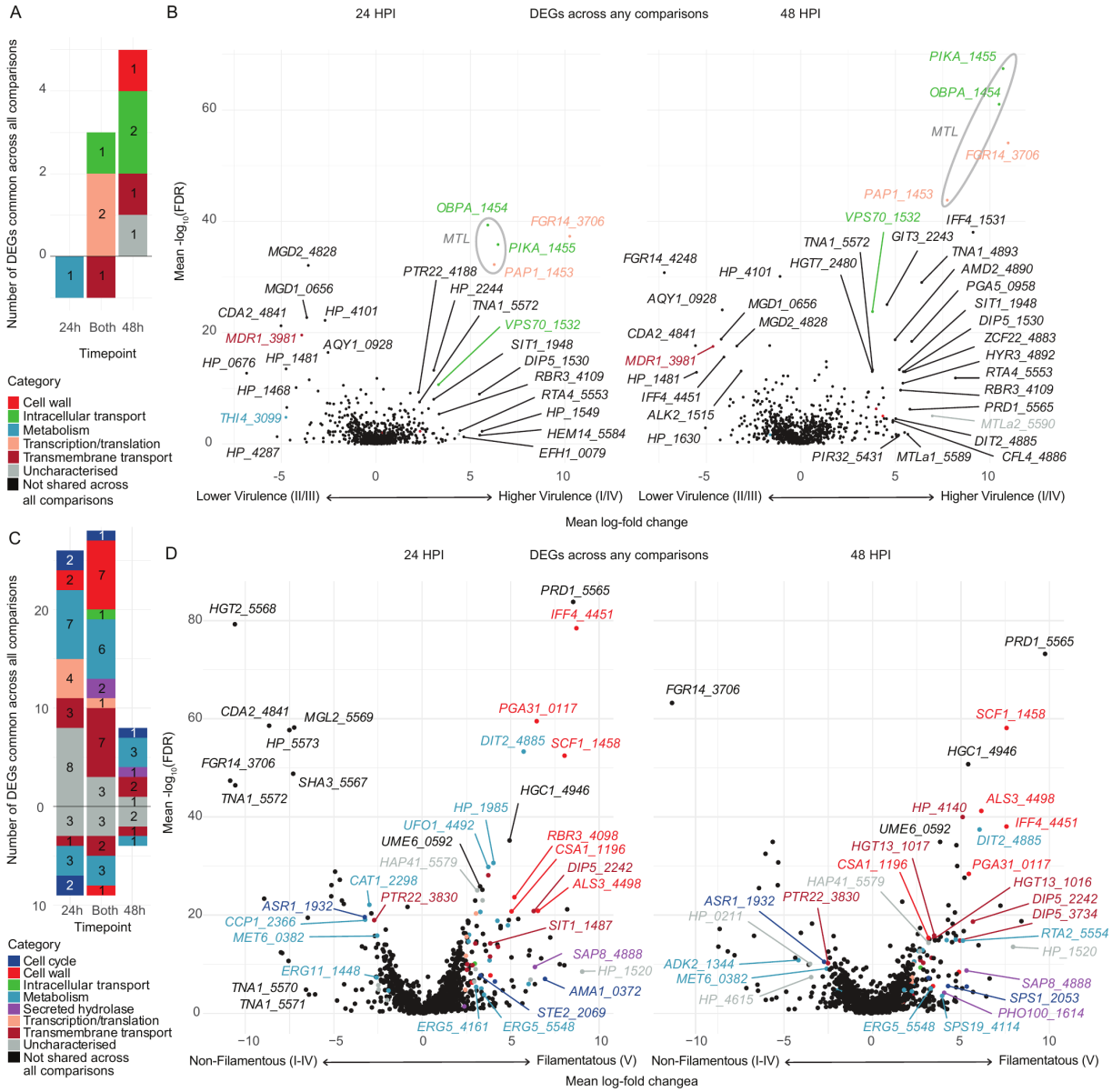

Figure 4: Interclade comparisons for virulence and filamentation: (A): The set of differentially expressed genes (DEGs) shared across all comparisons between clade I and IV (more virulent) and clade II and III (less virulent), coloured by manually annotated category, at either 24 or 48 h post infection (HPI). **(B)** Volcano plots

1337 demonstrate mean log-fold change for each DEG found in any comparison; genes
1338 included in the combined set are coloured as per **A**. **(C)** The set of DEGs shared across
1339 all comparisons between filamenting clade V all other clades (I-IV) *in vivo*, coloured by
1340 manually annotated category. **(D):** Volcano plots demonstrating mean log-fold change
1341 for all comparisons between clade V and clades I-IV at 24 HPI and 48 HPI for each
1342 DEG found in any comparison; genes included in the combined set are coloured as per
1343 **C**.

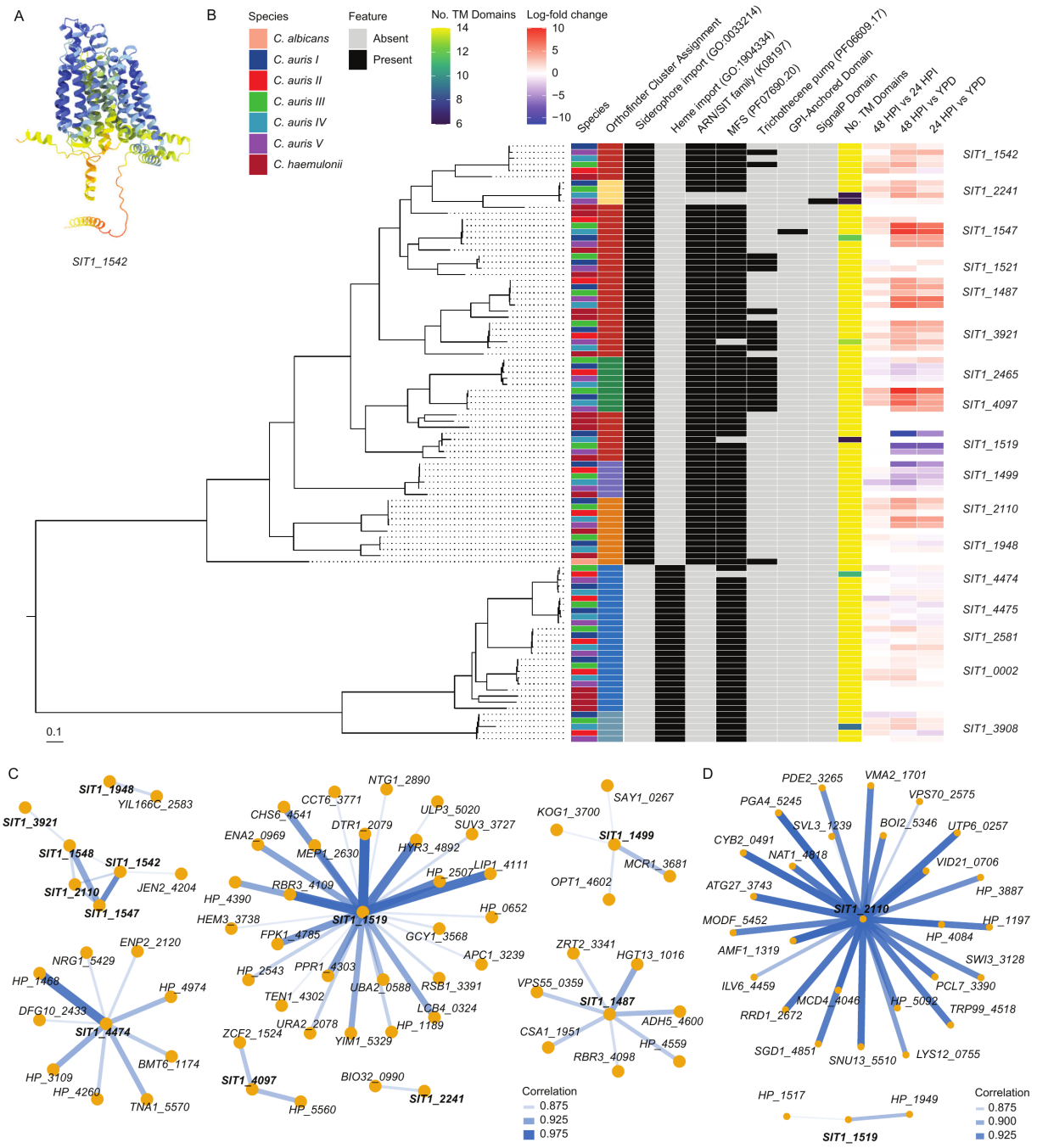

1344

1345 **Figure 5. Xenosiderophore Transporter Analysis: (A)** AlphaFold 3 predicted protein
1346 folding for peptide sequences for a xenosiderophore transporter candidate, illustrating
1347 the conserved 14-transmembrane domain similarity across the families. **(B)** RAXML
1348 phylogeny using 1000 bootstraps and LG4X model of Muscle-aligned protein

1349 sequences for orthologues of *C. albicans* Siderophore Transport 1 *SIT1* gene. Scale bar
1350 indicates number of substitutions per site. Orthofinder cluster assignment notes which
1351 grouping each gene was assigned to by our Synima/Orthofinder pipeline. **(C)** Pearson's
1352 correlation co-expression of associated gene expression involving siderophore transport
1353 candidate genes. **(D)** Pearson's correlation co-expression across available RNA-seq
1354 data from meta-analysis of 35 studies (**Table S4**), demonstrating a different set of
1355 transcriptional co-expression indicated by external experimental data.

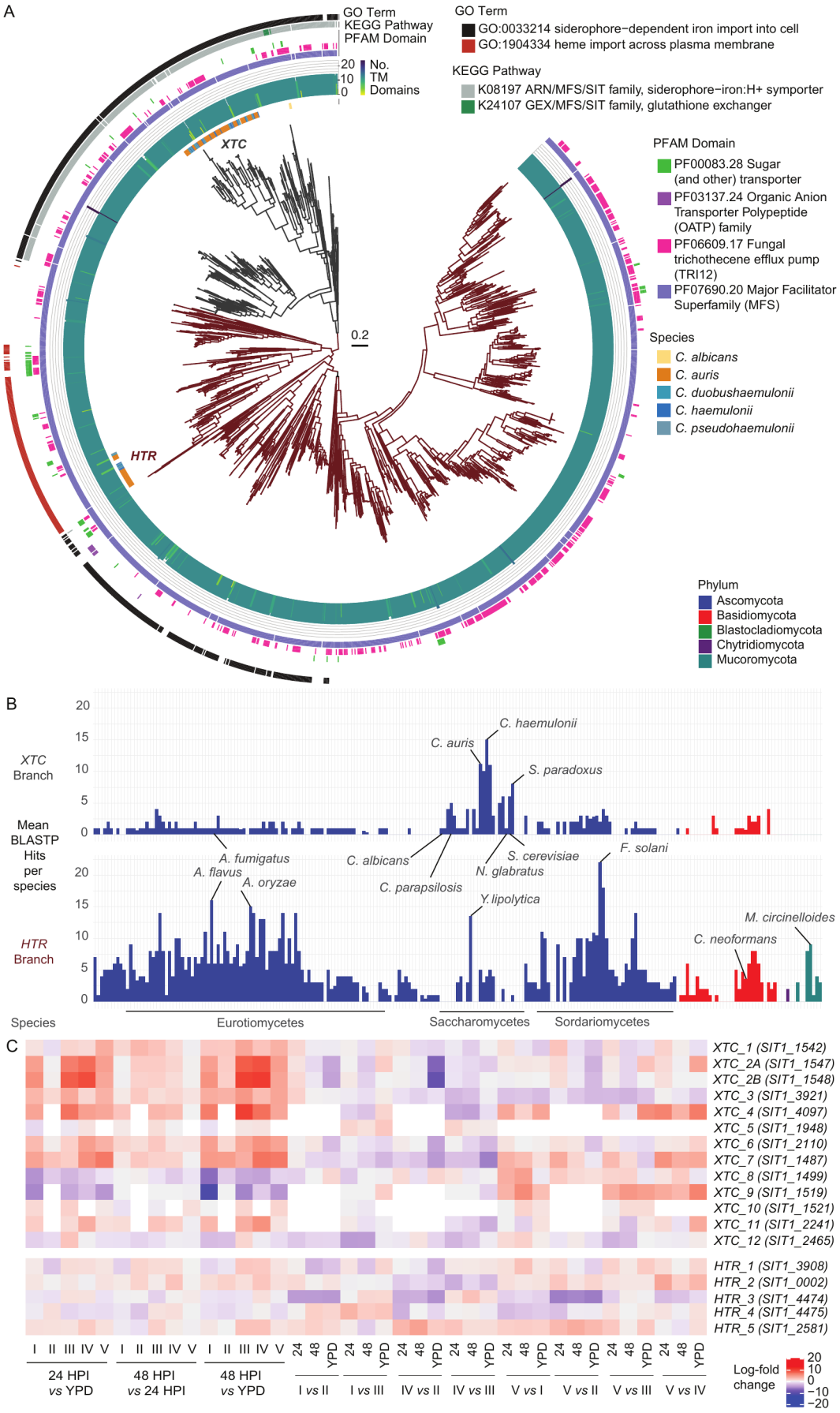
A
GO Term
KEGG Pathway
PFAM Domain
20
10
0
No. TM Domains
XTC
HTR
0.2
GO Term
GO:0033214 siderophore−dependent iron import into cell
GO:1904334 heme import across plasma membrane
KEGG Pathway
K08197 ARN/MFS/SIT family, siderophore−iron:H+ symporter
K24107 GEX/MFS/SIT family, glutathione exchanger
PFAM Domain
PF00083.28 Sugar (and other) transporter
PF03137.24 Organic Anion Transporter Polypeptide (OATP) family
PF06609.17 Fungal trichothecene efflux pump (TRI12)
PF07690.20 Major Facilitator Superfamily (MFS)
Species
C. albicans
C. auris
C. duobushaemulonii
C. haemulonii
C. pseudohaemulonii
Phylum
Ascomycota
Basidiomycota
Blastocladiomycota
Chytridiomycota
Mucoromycota
B
XTC Branch
Mean BLASTP Hits per species
HTR Branch
Species
C. haemulonii
C. auris
S. paradoxus
A. fumigatus
A. flavus
A. oryzae
C. albicans
C. parapsilosis
S. cerevisiae
N. glabratus
Y. lipolytica
F. solani
M. circinelloides
C. neoformans
Eurotiomycetes
Saccharomycetes
Sordariomycetes
C
XTC_1 (SIT1_1542)
XTC_2A (SIT1_1547)
XTC_2B (SIT1_1548)
XTC_3 (SIT1_3921)
XTC_4 (SIT1_4097)
XTC_5 (SIT1_1948)
XTC_6 (SIT1_2110)
XTC_7 (SIT1_1487)
XTC_8 (SIT1_1499)
XTC_9 (SIT1_1519)
XTC_10 (SIT1_1521)
XTC_11 (SIT1_2241)
XTC_12 (SIT1_2465)
HTR_1 (SIT1_3908)
HTR_2 (SIT1_0002)
HTR_3 (SIT1_4474)
HTR_4 (SIT1_4475)
HTR_5 (SIT1_2581)
24 HPI vs YPD
48 HPI vs 24 HPI
48 HPI vs YPD
I vs II
I vs III
IV vs II
IV vs III
V vs I
V vs II
V vs III
V vs IV
Log-fold change

1357 **Figure 6. Panfungal Xenosiderophore Phylogeny: (A)** Phylogeny of Blastp hits for
1358 *C. albicans SIT1* across fungal genomes available in FungiDB. Sequences were aligned
1359 with Clustal Omega and FastTree, scale bar shows substitutions per site. Two main
1360 branches emerged, a xenosiderophore transporter candidate branch (*XTC*) and a haem
1361 transport-related branch (*HTR*), based mainly on the GO terms assigned (outer ring).
1362 **(B)** Bar chart depicting per-species mean Blastp hits for siderophore transporters. **(C)**
1363 Heatmap of all DEGs across comparisons in this paper for each *XTC* and *HTR* gene,
1364 assigned in order of contig in the B8441 v3 reference genome. White spaces represent
1365 clades where each orthologue was not found in Orthofinder (*XTC4*, *XTC9* and *XTC11* in
1366 clade II, *XTC5* in II and V, *XTC10* in II and IV, **Fig. 5B**).

Supplementary Figures

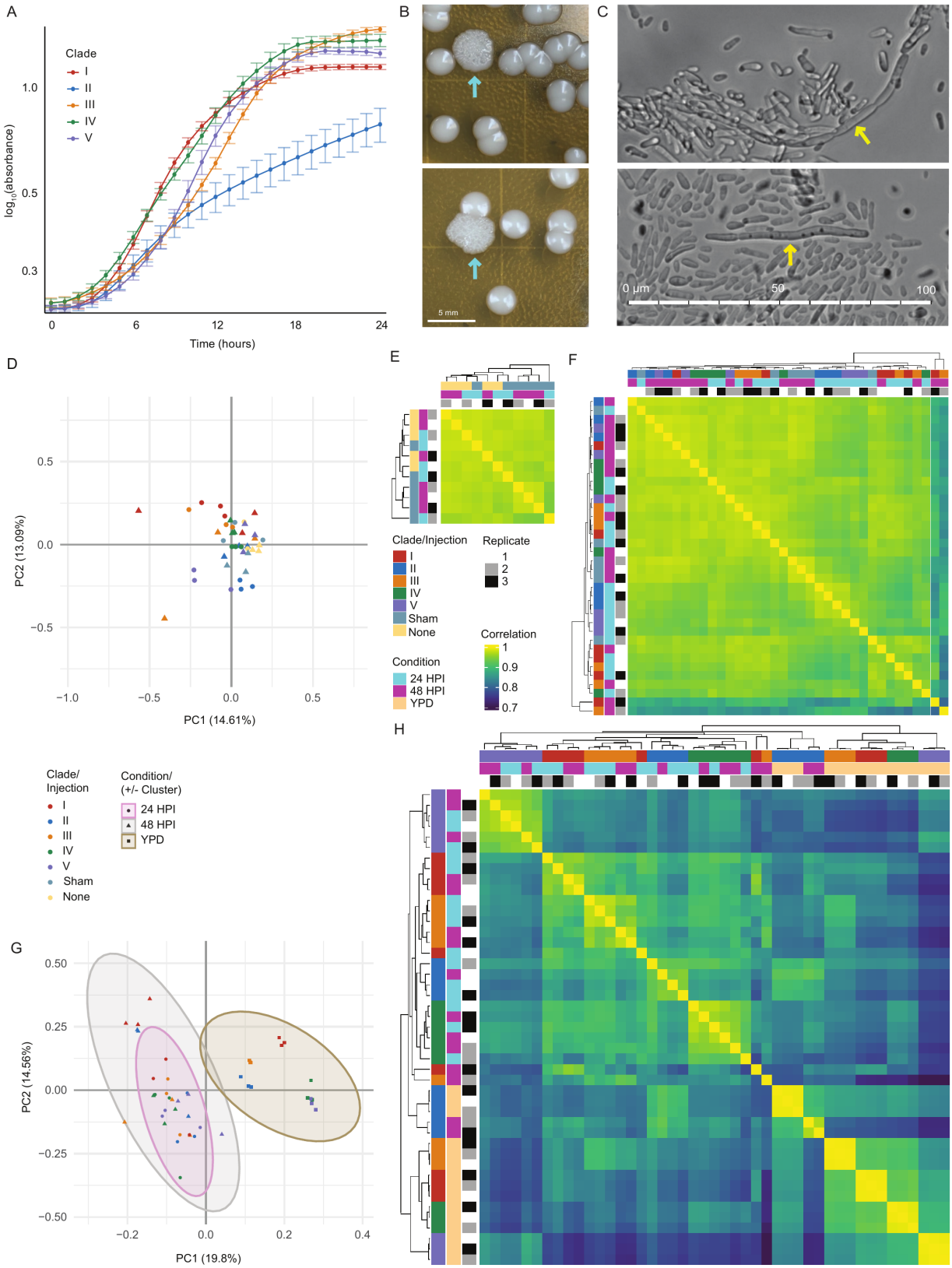
A
Clade
I
II
III
IV
V
log10(absorbance)
1.0
0.5
0.3
0
6
12
18
24
Time (hours)
B
5 mm
C
0 µm
50
100
D
PC2 (13.09%)
PC1 (14.61%)
Clade/
Injection
Condition/
(+/- Cluster)
24 HPI
48 HPI
YPD
Sham
None
E
Clade/Injection
Replicate
Condition
Correlation
F
G
PC2 (14.56%)
PC1 (19.8%)
H

1370 **Supplementary Figure 1:** Profiles of *C. auris* growth, morphotype, morphology, and
1371 gene expression. **(A)** Growth curves for five representative strains of *C. auris* over 24 h
1372 *in vitro*. **(B)** Rough colonies demonstrated on YPD-agar after recovery from AK infection
1373 in clade V only (blue arrows). **(C)** Filamentous forms (yellow arrows) isolated from rough
1374 colonies and imaged on light microscopy in distilled de-ionised water. **(D)** Principle
1375 components analysis (PCA) of fragments per kilobase per million (FPKM) gene
1376 expression for AK host transcription. **(E)** Correlation matrix for individual replicates' log_2-
1377 transformed transcript counts per million for AK responses to sham injection and no
1378 injection **(F)** Correlation matrix as above for AK responses to *C. auris* infection and
1379 sham injection. **(G)** PCA of FPKM gene expression for *C. auris* pathogen transcription.
1380 **(H)** Correlation matrix as above for *C. auris* gene expression *in vivo* and *in vivo* across
1381 five clades.

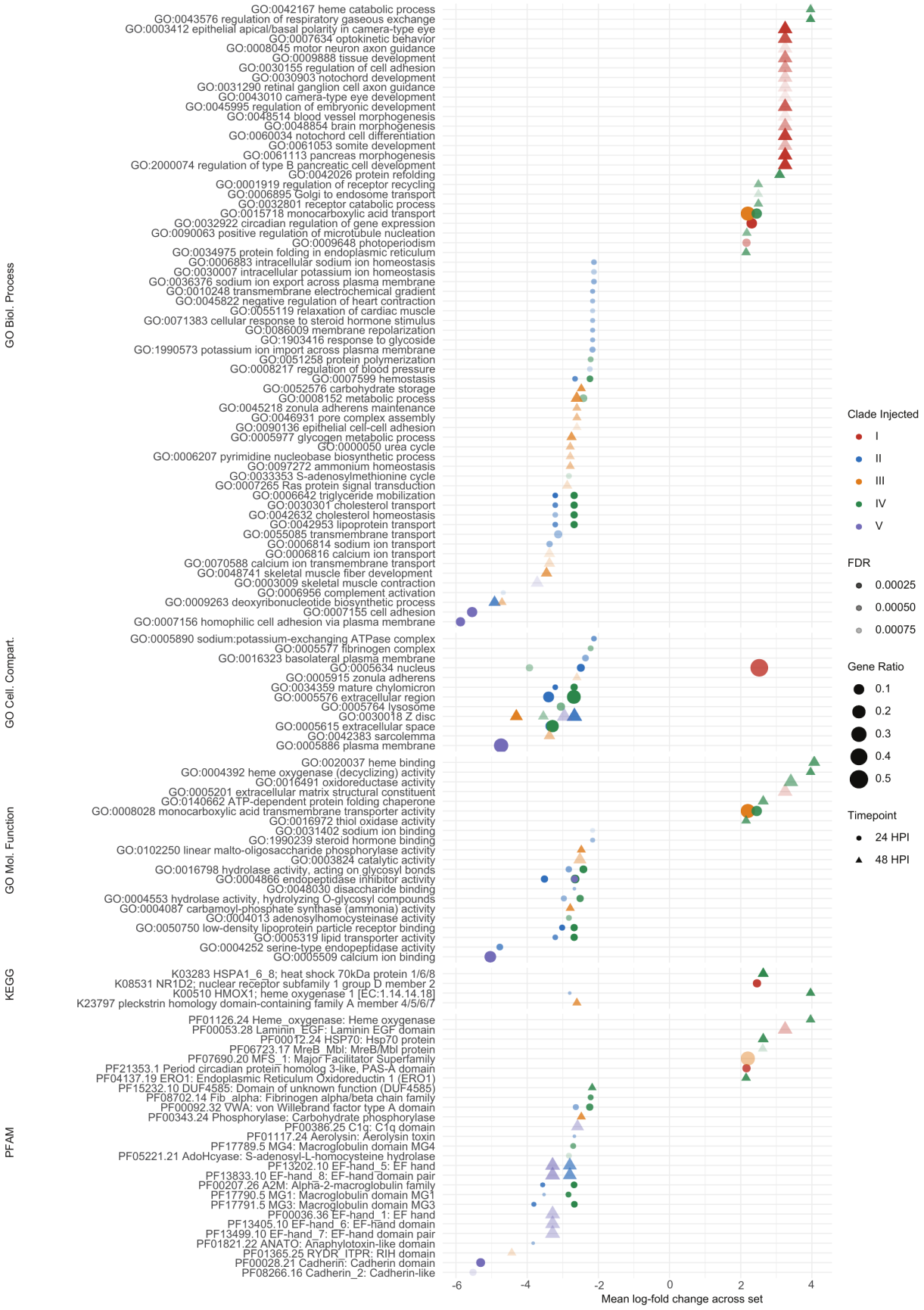
GO Biol. Process
GO:0042167 heme catabolic process
GO:0043576 regulation of respiratory gaseous exchange
GO:0003412 epithelial apical/basal polarity in camera-type eye
GO:0007634 optokinetic behavior
GO:0008045 motor neuron axon guidance
GO:0009888 tissue development
GO:0030155 regulation of cell adhesion
GO:0030903 notochord development
GO:0031290 retinal ganglion cell axon guidance
GO:0043010 camera-type eye development
GO:0045995 regulation of embryonic development
GO:0048514 blood vessel morphogenesis
GO:0048854 brain morphogenesis
GO:0060034 notochord cell differentiation
GO:0061053 somite development
GO:0061113 pancreas morphogenesis
GO:2000074 regulation of type B pancreatic cell development
GO:0042026 protein refolding
GO:0001919 regulation of receptor recycling
GO:0006895 Golgi to endosome transport
GO:0032801 receptor catabolic process
GO:0015718 monocarboxylic acid transport
GO:0032922 circadian regulation of gene expression
GO:0090063 positive regulation of microtubule nucleation
GO:0009648 photoperiodism
GO:0034975 protein folding in endoplasmic reticulum
GO:0006883 intracellular sodium ion homeostasis
GO:0030007 intracellular potassium ion homeostasis
GO:0036376 sodium ion export across plasma membrane
GO:0010248 transmembrane electrochemical gradient
GO:0045822 negative regulation of heart contraction
GO:0055119 relaxation of cardiac muscle
GO:0071383 cellular response to steroid hormone stimulus
GO:0086009 membrane repolarization
GO:1903416 response to glycoside
GO:1990573 potassium ion import across plasma membrane
GO:0051258 protein polymerization
GO:0008217 regulation of blood pressure
GO:0007599 hemostasis
GO:0052576 carbohydrate storage
GO:0008152 metabolic process
GO:0045218 zonula adherens maintenance
GO:0046931 pore complex assembly
GO:0090136 epithelial cell-cell adhesion
GO:0005977 glycogen metabolic process
GO:0000050 urea cycle
GO:0006207 pyrimidine nucleobase biosynthetic process
GO:0097272 ammonium homeostasis
GO:0033353 S-adenosylmethionine cycle
GO:0007265 Ras protein signal transduction
GO:0006642 triglyceride mobilization
GO:0030301 cholesterol transport
GO:0042632 cholesterol homeostasis
GO:0042953 lipoprotein transport
GO:0055085 transmembrane transport
GO:0006814 sodium ion transport
GO:0006816 calcium ion transport
GO:0070588 calcium ion transmembrane transport
GO:0048741 skeletal muscle fiber development
GO:0003009 skeletal muscle contraction
GO:0006956 complement activation
GO:0009263 deoxyribonucleotide biosynthetic process
GO:0007155 cell adhesion
GO:0007156 homophilic cell adhesion via plasma membrane
GO Cell. Compart.
GO:0005890 sodium:potassium-exchanging ATPase complex
GO:0005577 fibrinogen complex
GO:0016323 basolateral plasma membrane
GO:0005634 nucleus
GO:0005915 zonula adherens
GO:0034359 mature chylomicron
GO:0005576 extracellular region
GO:0005764 lysosome
GO:0030018 Z disc
GO:0005615 extracellular space
GO:0042383 sarcolemma
GO:0005886 plasma membrane
GO Mol. Function
GO:0020037 heme binding
GO:0004392 heme oxygenase (decyclizing) activity
GO:0016491 oxidoreductase activity
GO:0005201 extracellular matrix structural constituent
GO:0140662 ATP-dependent protein folding chaperone
GO:0008028 monocarboxylic acid transmembrane transporter activity
GO:0016972 thiol oxidase activity
GO:0031402 sodium ion binding
GO:1990239 steroid hormone binding
GO:0102250 linear malto-oligosaccharide phosphorylase activity
GO:0003824 catalytic activity
GO:0016798 hydrolase activity, acting on glycosyl bonds
GO:0004866 endopeptidase inhibitor activity
GO:0048030 disaccharide binding
GO:0004553 hydrolase activity, hydrolyzing O-glycosyl compounds
GO:0004087 carbamoyl-phosphate synthase (ammonia) activity
GO:0004013 adenosylhomocysteinase activity
GO:0050750 low-density lipoprotein particle receptor binding
GO:0005319 lipid transporter activity
GO:0004252 serine-type endopeptidase activity
GO:0005509 calcium ion binding
KEGG
K03283 HSPA1_6_8; heat shock 70kDa protein 1/6/8
K08531 NR1D2; nuclear receptor subfamily 1 group D member 2
K00510 HMOX1; heme oxygenase 1 [EC:1.14.14.18]
K23797 pleckstrin homology domain-containing family A member 4/5/6/7
PFAM
PF01126.24 Heme_oxygenase: Heme oxygenase
PF00053.28 Laminin_EGF: Laminin EGF domain
PF00012.24 HSP70: Hsp70 protein
PF06723.17 MreB_Mbl: MreB/Mbl protein
PF07690.20 MFS_1: Major Facilitator Superfamily
PF21353.1 Period circadian protein homolog 3-like, PAS-A domain
PF04137.19 ERO1: Endoplasmic Reticulum Oxidoreductin 1 (ERO1)
PF15232.10 DUF4585: Domain of unknown function (DUF4585)
PF08702.14 Fib_alpha: Fibrinogen alpha/beta chain family
PF00092.32 VWA: von Willebrand factor type A domain
PF00343.24 Phosphorylase: Carbohydrate phosphorylase
PF00386.25 C1q: C1q domain
PF01117.24 Aerolysin: Aerolysin toxin
PF17789.5 MG4: Macroglobulin domain MG4
PF05221.21 AdoHcyase: S-adenosyl-L-homocysteine hydrolase
PF13202.10 EF-hand_5: EF hand
PF13833.10 EF-hand_8: EF-hand domain pair
PF00207.26 A2M: Alpha-2-macroglobulin family
PF17790.5 MG1: Macroglobulin domain MG1
PF17791.5 MG3: Macroglobulin domain MG3
PF00036.36 EF-hand_1: EF hand
PF13405.10 EF-hand_6: EF-hand domain
PF13499.10 EF-hand_7: EF-hand domain pair
PF01821.22 ANATO: Anaphylotoxin-like domain
PF01365.25 RYDR_ITPR: RIH domain
PF00028.21 Cadherin: Cadherin domain
PF08266.16 Cadherin_2: Cadherin-like
-6
-4
-2
0
2
4
Mean log-fold change across set
Clade Injected
I
II
III
IV
V
FDR
0.00025
0.00050
0.00075
Gene Ratio
0.1
0.2
0.3
0.4
0.5
Timepoint
24 HPI
48 HPI

1383 **Supplementary Figure 2: *A. dispar* gene ontology, pathway and domain**
1384 **enrichment during infection *vs* sham control:** The GJEY01 *A. dispar* transcripts
1385 were annotated for Gene Ontology (GO) terms using DIAMOND2GO, Kyoto
1386 Encycopaedia of Genes and Genome pathways using BLASTKoala, and PFAM
1387 domains using HMMScan. For each set of up-regulated or down-regulated genes in
1388 each comparison between an injected *C. auris* clade and sham injection, Fisher's exact
1389 test was used with Benjamini-Hochberg (BH) correction for multiple testing for each set,
1390 with a false discovery rate (FDR) cut-off of 0.001. Mean log-fold change and ratio of
1391 genes in that set was calculated for genes in each set possessing each feature.
1392 Redundant GO terms were removed using Revigo.

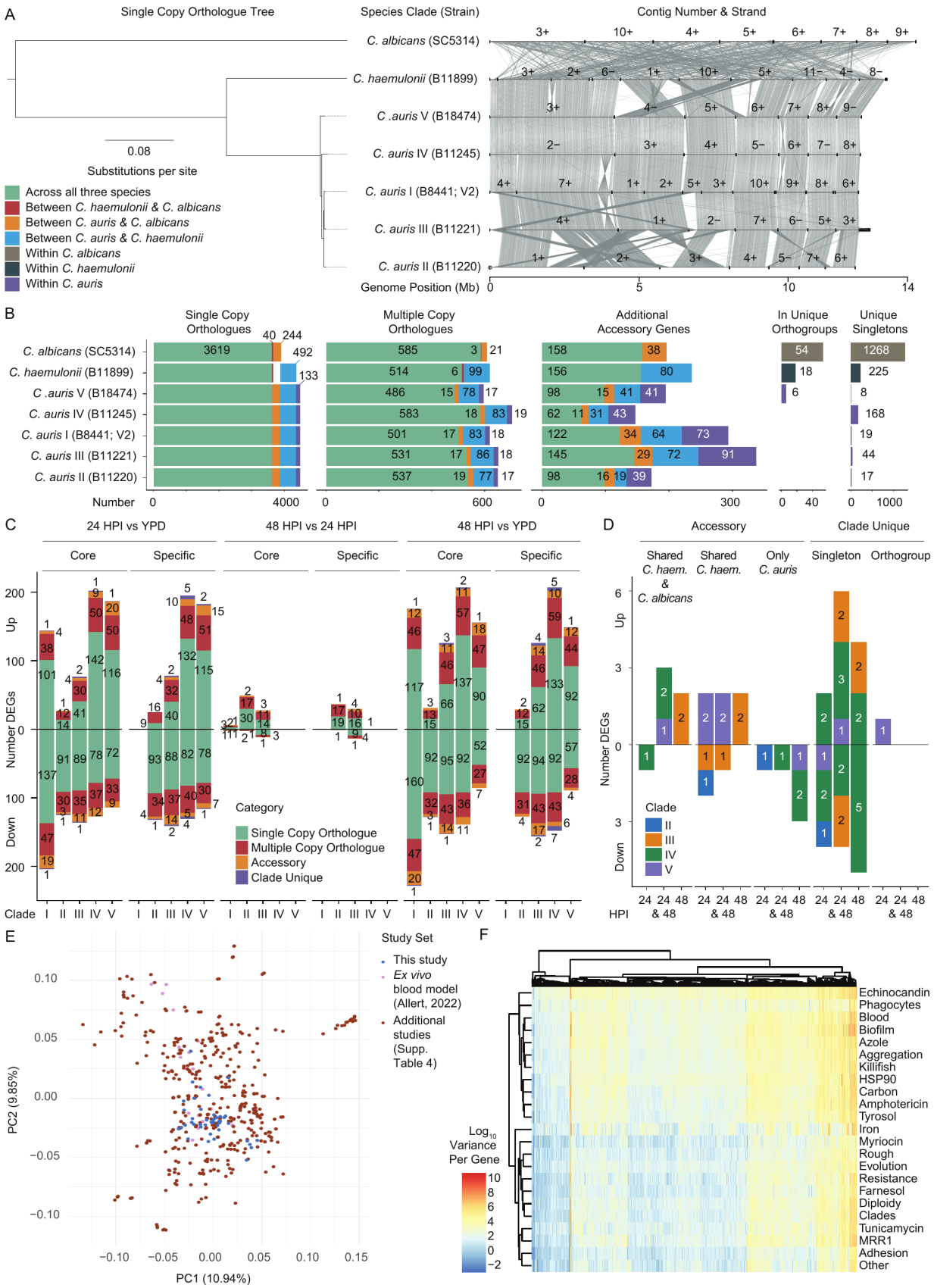
A
Single Copy Orthologue Tree
Species Clade (Strain)
Contig Number & Strand
C. albicans (SC5314)
C. haemulonii (B11899)
C .auris V (B18474)
C. auris IV (B11245)
C. auris I (B8441; V2)
C. auris III (B11221)
C. auris II (B11220)
Genome Position (Mb)
0.08
Substitutions per site
Across all three species
Between C. haemulonii & C. albicans
Between C. auris & C. albicans
Between C. auris & C. haemulonii
Within C. albicans
Within C. haemulonii
Within C. auris
B
Single Copy Orthologues
Multiple Copy Orthologues
Additional Accessory Genes
In Unique Orthogroups
Unique Singletons
Number
C
24 HPI vs YPD
48 HPI vs 24 HPI
48 HPI vs YPD
Core
Specific
Up
Down
Number DEGs
Clade
Category
Single Copy Orthologue
Multiple Copy Orthologue
Accessory
Clade Unique
D
Accessory
Clade Unique
Shared C. haem. & C. albicans
Shared C. haem.
Only C. auris
Singleton
Orthogroup
Clade
II
III
IV
V
HPI
E
Study Set
This study
Ex vivo blood model (Allert, 2022)
Additional studies (Supp. Table 4)
PC2 (9.85%)
PC1 (10.94%)
F
Log10 Variance Per Gene
Echinocandin
Phagocytes
Blood
Biofilm
Azole
Aggregation
Killifish
HSP90
Carbon
Amphotericin
Tyrosol
Iron
Myriocin
Rough
Evolution
Resistance
Farnesol
Diploidy
Clades
Tunicamycin
MRR1
Adhesion
Other

1394 **Supplementary Figure 3. Contextualising differential gene expression across**
1395 **orthogroups and broder RNA-seq datasets. (A)** Single copy orthologue phylogeny
1396 and Synima/Orthofinder synteny plot of reference genomes for *C. albicans,*
1397 *C. haemulonii* and the five clades of *C. auris* used in this study. Despite many
1398 orthologues, there is little synteny with *C. albicans*; prominent translocations and
1399 inversions are seen between *C. haemulonii* and *C. auris*, and for clade II. **(B)** Counts
1400 are shown for orthologues contained within and between species, whether single copy
1401 or multiple copy, with additional counts for accessory genomes. Clade V is the only
1402 *C. auris* clade with a single orthogroup, containing six genes, while clade IV has the
1403 highest number of apparently unique genes that were not assigned to any orthogroup.
1404 **(C)** Differential gene expression for *in vivo vs in vitro* comparisons, comparing numbers
1405 of DEGs identified when using a single core reference genome (B8441, clade I) or a
1406 clade-specific reference genome for each individual clade. **(D)** Differential expression of
1407 specific genes not present in core reference genome. **(E)** RNA-seq meta-analysis. 36
1408 public datasets were identified for *C. auris* transcriptome expression and assessed for
1409 variance by PCA dimensionality reduction of normalised expression of single copy
1410 orthologues, indicating AK dataset clusters similarly to experiments using an *ex vivo*
1411 blood model and other experiments. **(F)** Hierarchical clustering of per-gene variance,
1412 calculated for all B8441 core genes for each study, demonstrating similar clustering and
1413 profile of within-experiment variance per gene.

Down
Up
24 HPI
48 HPI
24 vs YPD
48 vs 24
48 vs YPD
GO Biol. Process
GO:0034219: carbohydrate transmembrane transport
GO:0008643: carbohydrate transport
GO:0097080: plasma membrane selenite transport
GO:0006811: monoatomic ion transport
GO:0035433: acetate transmembrane transport
GO:0019740: nitrogen utilization
GO:0072488: ammonium transmembrane transport
GO:0006544: glycine metabolic process
GO:0000027: ribosomal large subunit assembly
GO:0006412: translation
GO:0002181: cytoplasmic translation
GO:0006825: copper ion transport
GO:0051156: glucose 6−phosphate metabolic process
GO:0046835: carbohydrate phosphorylation
GO:0008202: steroid metabolic process
GO:0006629: lipid metabolic process
GO:0006044: N−acetylglucosamine metabolic process
GO:0005975: carbohydrate metabolic process
GO:0006260: DNA replication
GO:0006694: steroid biosynthetic process
GO:0044088: regulation of vacuole organization
GO:0009251: glucan catabolic process
GO:0030174: regulation of DNA−templated DNA replication initiation
GO:0051515: positive regulation of monopolar cell growth
GO:0061091: regulation of phospholipid translocation
GO:0035672: oligopeptide transmembrane transport
GO:1903710: spermine transmembrane transport
GO:0071555: cell wall organization
GO:0000103: sulfate assimilation
GO:0030447: filamentous growth
GO Cell. Compart.
GO:0016020: membrane
GO:0005575: cellular_component
GO:0000324: fungal−type vacuole
GO:0031410: cytoplasmic vesicle
GO:0005886: plasma membrane
GO:0005737: cytoplasm
GO:0005829: cytosol
GO:0005634: nucleus
GO:0005960: glycine cleavage complex
GO:1990904: ribonucleoprotein complex
GO:0005840: ribosome
GO:0071944: cell periphery
GO:0005656: nuclear pre−replicative complex
GO:0042555: MCM complex
GO:0071162: CMG complex
GO:0031966: mitochondrial membrane
GO:0009277: fungal−type cell wall
GO:0005576: extracellular region
GO Mol. Function
GO:0015578: mannose transmembrane transporter activity
GO:0005315: inorganic phosphate transmembrane transporter activity
GO:0016705: oxidoreductase activity (paired donors)
GO:0097079: selenite:proton symporter activity
GO:0004497: monooxygenase activity
GO:0015343: siderophore−iron transmembrane transporter activity
GO:0015123: acetate transmembrane transporter activity
GO:0022857: transmembrane transporter activity
GO:0000293: ferric−chelate reductase activity
GO:0003674: molecular_function
GO:0008519: ammonium transmembrane transporter activity
GO:0000166: nucleotide binding
GO:0030527: structural constituent of chromatin
GO:0046982: protein heterodimerization activity
GO:0016740: transferase activity
GO:0019843: rRNA binding
GO:0003723: RNA binding
GO:0016773: phosphotransferase activity, alcohol group as acceptor
GO:0005536: glucose binding
GO:0019158: mannokinase activity
GO:0003697: single−stranded DNA binding
GO:0016491: oxidoreductase activity
GO:0017116: single−stranded DNA helicase activity
GO:0003688: DNA replication origin binding
GO:0020037: heme binding
GO:0000297: spermine transmembrane transporter activity
GO:0035673: oligopeptide transmembrane transporter activity
GO:0004190: aspartic−type endopeptidase activity
KEGG
K08139: HXT; MFS transporter, SP family, sugar:H+ symporter
K08197: ARN; MFS transporter, SIT family, siderophore−iron:H+ symporter
K08192: DAL5; MFS transporter, ACS family, DAL5 transporter family protein
K07034: K07034; uncharacterized protein
K11253: H3; histone H3
K11251: H2A; histone H2A
K00844: HK; hexokinase [EC:2.7.1.1]
K06005: SAP; candidapepsin [EC:3.4.23.24]
PFAM
PF15789.9: Hyr1: Hyphally regulated cell wall GPI−anchored protein 1
PF11765.12: Hyphal_reg_CWP: Hyphally regulated cell wall protein N−terminal
PF01425.25: Amidase: Amidase
PF00083.28: Sugar_tr: Sugar (and other) transporter
PF00067.26: p450: Cytochrome P450
PF07738.17: Sad1_UNC: Sad1 / UNC−like C−terminal
PF03583.18: LIP: Secretory lipase
PF12988.11: TraQ_transposon: TraQ conjugal transfer protein
PF15580.10: Imm53: Immunity protein 53
PF05730.15: CFEM: CFEM domain
PF08030.16: NAD_binding_6: Ferric reductase NAD binding domain
PF01184.23: Gpr1_Fun34_YaaH: GPR1/FUN34/yaaH family
PF01794.23: Ferric_reduct: Ferric reductase like transmembrane component
PF08022.16: FAD_binding_8: FAD−binding domain
PF07690.20: MFS_1: Major Facilitator Superfamily
PF00125.28: Histone: Core histone H2A/H2B/H3/H4
PF00428.23: Ribosomal_60s: 60s Acidic ribosomal protein
PF16211.9: Histone_H2A_C: C−terminus of histone H2A
PF06609.17: TRI12: Fungal trichothecene efflux pump (TRI12)
PF00349.25: Hexokinase_1: Hexokinase
PF03727.20: Hexokinase_2: Hexokinase
PF00493.27: MCM: MCM P−loop domain
PF01078.25: Mg_chelatase: Magnesium chelatase, subunit ChlI
PF14551.10: MCM_N: MCM N−terminal domain
PF17207.7: MCM_OB: MCM OB domain
PF17855.5: MCM_lid: MCM AAA−lid domain
PF03169.19: OPT: OPT oligopeptide transporter protein
PF00026.27: Asp: Eukaryotic aspartyl protease
Other
Accessory
NetGPI: GPI−Anchored
DeepTMM Predicted TM−domain(s)
SignalP5: SP(Sec/SPI)
FDR
0.00025
0.00050
0.00075
Ratio
0.2
0.4
0.6
Mean log-fold change
10
5
0
−5
I IV V V V V I I IV V V V V V I III IV V III I II III IV V I I IV V V V V V I I IV V V V V V I II III IV V I II III
vs
II II III I II III IV II III II III I II III IV II III II III I II III IV II III II III I II III IV
Clade Comparison

1415 **Supplementary Figure 4. *C. auris* Gene Set, Pathway and Domain Enrichment:**
1416 Transcripts from *C. auris* reference genomes for each clade were annotated for Gene
1417 Ontology (GO) terms using DIAMOND2GO, Kyoto Encycopaedia of Genes and
1418 Genome pathways using BLASTKoala, PFAM domains using HMMScan,
1419 transemembrane domains with DeepTMHMM, GPI-anchored domains with NetGPI,
1420 SignalP domains with SignalP5, and membership within the accessory genome using
1421 Synima/Orthofinder. For each set of up-regulated or down-regulated genes in each
1422 comparison, Fisher's exact test was used with Benjamini-Hochberg (BH) correction for
1423 multiple testing for each set, with a false discovery rate (FDR) cut-off of 0.001. Mean
1424 log-fold change and ratio of genes in that set was calculated for genes in each set
1425 possessing each feature.

1426

1427 **Supplementary Figure 5. *C. auris* Mating-Type Locus Gene Expression: (A)**
1428 Transcripts (fragments per kilobase per million, FPKM) for orthogroups aligned to the
1429 same reference genome (left-hand panels) and clade-specific reference genomes (right-
1430 hand panels), indicating similar transcript levels between clades for e.g. *PIKA*, *OBPA*
1431 and *PAP1* non-mating genes when aligned to clade-specific reference genomes. **(B)**
1432 Comparing individual transcript levels for each orthogroup in more *vs* less virulent
1433 clades *via* Wilcoxon signed-rank test with Bonferroni correction to minimise false
1434 positives, demonstrating that only down-regulation of *THI4* (at 24 HPI), *MRD1* (at both
1435 time-points), and up-regulation of *PGA30* and *PIKA* were significantly different.

1436 Significance levels are as follows: * p <= 0.05, ** <= 0.01, *** <= 0.001, **** <= 0.0001,

1437 ***** <= 0.00001.

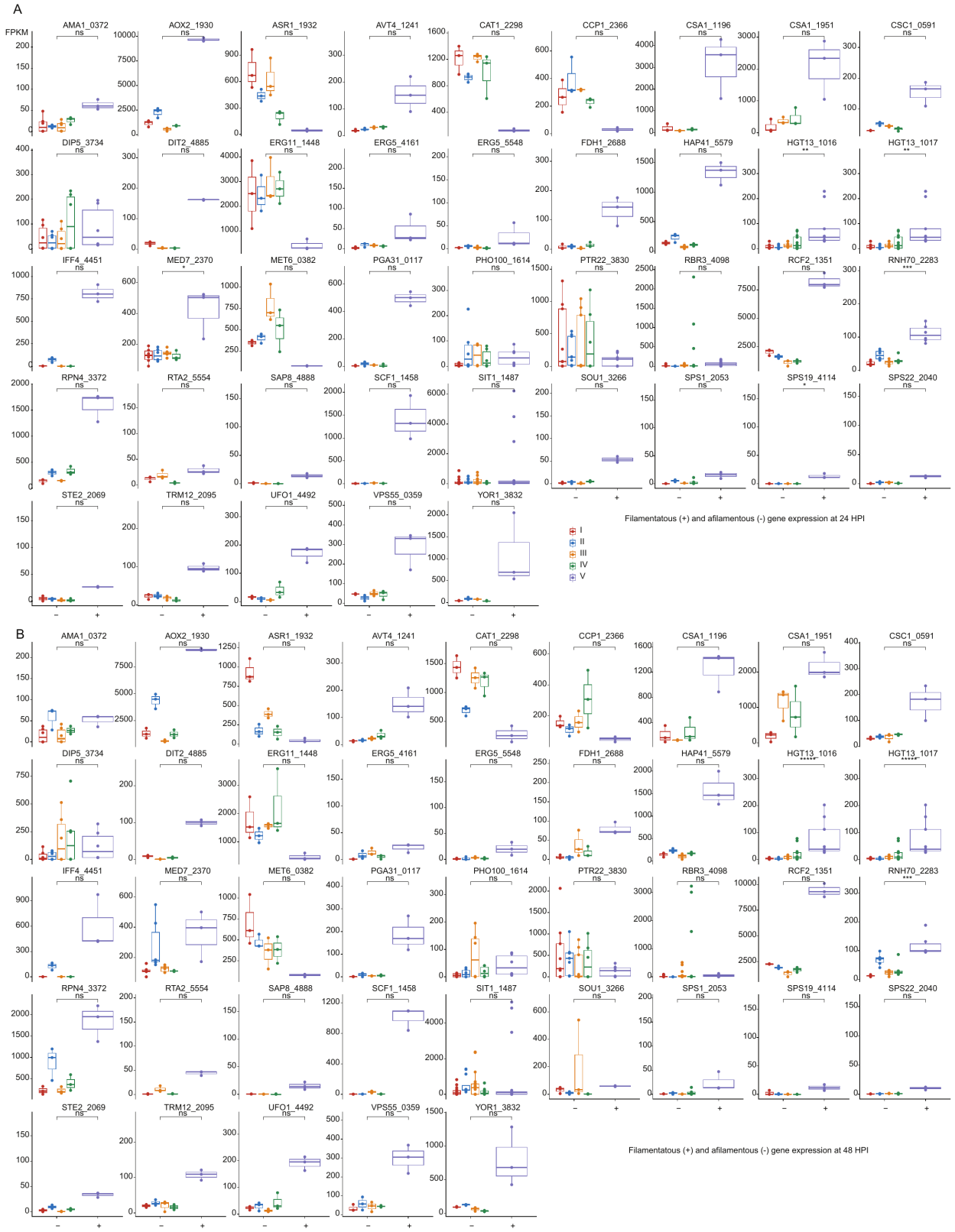
A
FPKM
AMA1_0372
AOX2_1930
ASR1_1932
AVT4_1241
CAT1_2298
CCP1_2366
CSA1_1196
CSA1_1951
CSC1_0591
DIP5_3734
DIT2_4885
ERG11_1448
ERG5_4161
ERG5_5548
FDH1_2688
HAP41_5579
HGT13_1016
HGT13_1017
IFF4_4451
MED7_2370
MET6_0382
PGA31_0117
PHO100_1614
PTR22_3830
RBR3_4098
RCF2_1351
RNH70_2283
RPN4_3372
RTA2_5554
SAP8_4888
SCF1_1458
SIT1_1487
SOU1_3266
SPS1_2053
SPS19_4114
SPS22_2040
STE2_2069
TRM12_2095
UFO1_4492
VPS55_0359
YOR1_3832
Filamentatous (+) and afilamentous (-) gene expression at 24 HPI
I
II
III
IV
V
B
Filamentatous (+) and afilamentous (-) gene expression at 48 HPI

1438

1439 **Supplementary Figure 6: (A-B)** Comparing individual transcript levels for each
1440 orthogroup in filamentous clade V *vs* all other clades *via* Wilcoxon signed-rank test with
1441 Bonferroni correction to minimise false positives, demonstrating at 24 HPI **(A)** and
1442 48 HPI **(B)**, excluding any genes that were assigned to be "hypothetical proteins" only,
1443 up-regulation of two *HGT13* orthologues and *RNH70* were significantly different at both
1444 time-points, with up-regulation of *MED7* and *SPS19* at 24 HPI. Significance levels are
1445 as follows: * p <= 0.05, ** <= 0.01, *** <= 0.001, **** <= 0.0001, ***** <= 0.00001.
1446

1447 ## Supplementary Tables

1448

1449 **Supplementary Table 1. Clade-Representative *Candida auris* Strains Used In This**
1450 **Study:** Representative strain for each major clade of *C. auris* used in the study, with
1451 notes on human disease source, country of discovery, and date of isolation. Mortality
1452 statistics are given in terms of absolute numbers of embryos over biological triplicate
1453 experiments. Additional significance testing is also noted for pairwise comparisons by
1454 Log-Rank test with Benjamini-Hochberg (BH) correction.
1455

1456 **Supplementary Table 2: Differentially Expressed Genes in *A. dispar***
1457 **Microinjection:** All differentially expressed genes (DEGs) for *A. dispar* for (upper rows)
1458 sham injection *vs* no injection and (lower rows) *C. auris* injection *vs* sham injection.
1459 Gene IDs and descriptions follow annotations by Bonzi *et al.*[87]; log-fold change and -
1460 $\log_{10}$(false discovery rate) are calculated across all clades as a mean value for *C. auris*
1461 injection. Significant DEGs for each set of embryos injected with each clade are given
1462 (1 = significant, 0 = not significant), and the total number of clades where DEGs where
1463 significant is also given.
1464

1465 **Supplementary Table 3. Differentially Expressed Genes in *C. auris* Infection: (A)**
1466 Combined set of differentially expressed genes (DEGs) expressed by five clades during
1467 infection Each set of DEGs expressed *in vivo vs in vitro* for five clades was combined,

1468 resulting in a set of genes that were specific to *C. auris* infection at these timepoints. **(B)**
1469 Combined set of DEGs between more virulent and less virulent clades: Each set of
1470 DEGs between clades I & IV (more virulent) and II & III (less virulent) was compared at
1471 24 HPI and 48 HPI, resulting in a combined set expressed in infection. **(C)** Combined
1472 DEG Sets: between filamentous clade V and all other clades: Each set of DEGs
1473 between clade V and all each clades I-IV was compared at 24 HPI and 48 HPI, resulting
1474 in a combined set expressed in infection, excluding those significant during growth in
1475 YPD broth where clade V was not observed to filament. **(D)** Accessory genes not found
1476 in clade I reference genome: DEGs without orthologues in the clade I reference were
1477 identified and annotated. **(E)** Log-fold change and FDR across all pathogen gene
1478 expression. **(F)** Fragments per kilobase per million across all pathogen gene
1479 expression.
1480
1481 **Supplementary Table 4. Publicly available RNA-seq Data on 16th April 2024:** A
1482 systematic re-analysis of RNA expression across NCBI-available datasets for *C. auris*
1483 gene expression, categorised by research theme for analysis (**Fig. S1D-E**).
1484